Theory and Numerical Aspects of Constitutive Modeling in Finite Deformation Magnetomechanics

G. Ethiraj

Report/Preprint No. 09–I–04
Institut für Mechanik (Bauwesen) · Lehrstuhl I · Prof. C. Miehe
Universität Stuttgart, 70550 Stuttgart, Pfaffenwaldring 7, Germany

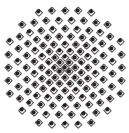

Contents

Acknowledgement

This thesis was conducted at the Institut für Mechanik (Bauwesen), Lehrstuhl I, Universität Stuttgart as part of the curriculum of the *Erasmus Mundus Master of Science in Computational Mechanics*, a joint initiative of the Universitat Politècnica de Catalunya (Barcelona, Spain), Swansea University (UK), Ecole Centrale Nantes (France) and the Universität Stuttgart (Germany) in cooperation with the *International Center for Numerical Methods in Engineering* (CIMNE).

I am grateful to Prof. Dr.-Ing. Christian Miehe for allowing me this opportunity and for his guidance. I would like to extend my heartfelt gratitude to my supervisor Bjoern Kiefer, Ph.D. from whom I have learnt a great deal not only in the topics covered in this theis but also from an overall perspective in research. I would also like to thank Dr. Antonio Orlando from Swansea University who got me interested in the field of Computational Mechanics.

I am greatly indebted to my family and friends who have been a constant source of encouragment throughout my studies. Last but not least, I would also like to take this opportunity to thank the European Commission for the Erasmus Mundus Program which funded me throughout the two years course without which it would never have been possible to work with eminent faculty and a rich research environment.

1. Introduction

In recent years, a number of industrial applications that make use of *magneto-sensitive materials* have been developed. *Magneto-sensitive elastomers* find use in controllable stiffness devices, controllable membranes and applications for active control of structural components and rapid response interfaces aimed at optimizing the performance of mechanical systems. These are a class of solids that consist of rubber matrix filled with micro- or nano-sized magnetizable particles such as iron. As a result, the mechanical properties of these materials can be varied by the application of magnetic field. This fact gives us a wide scope for their exploitation.

It is therefore of great interest to be able to reliably model or predict the properties of such materials by constitutive equations and present the solutions and analysis of representative boundary value problems. Also, since deformations of elastomers are typically quite large, there is an added need to develop the constitutive theory in a *finite strain context*.

The constitutive modeling of such materials has been the research interest of Hutter and van de Ven [15] and Eringen & Maugin [13] among others. Additionally finite element analysis for the numerical implementation of coupled boundary value problems is required. These aspects have been presented by Dorfmann & Ogden [10], Brigadnov & Dorfmann [3], Bustamante, Dorfmann & Ogden [4], Steinmann [33], Kankanala and Triantafyllidis [19] and Kiefer, Rosato & Miehe [21, 22] in both, small and large strain.

Modeling of materials cannot proceed without experimental results of response behavior and experimental observations like pictures of microstructure. Such experimental work has been presented in Jolly et al.[17], Davis[6], Varga Filipcsei & Zrínyi [31, 32].

1.1. Aim and Structure of the Thesis

The aim of this work is to study some aspects of modeling materials in a finite strain context, which exhibit magneto-mechanical coupling. We present here different types of free energy functions to model these materials. The free energy functions that are presented are motivated by the the experimental results and the knowledge of the microstructure of these materials. We also present an alternative form of the Finite Element implementation of such coupled magneto-mechanical coupled boundary value problems.

The second chapter gives an overview of the experimental knowledge and the microstructure of these materials. Here we identify the key features that we aim to capture, thus forming the motivation of the proposed models stated in Section 5.

In the third chapter, an introduction to continuum magnetomechanics is provided. Here, apart from the standard finite deformation equations, we introduce the magnetic field variables and their mapping properties along along with the balance principles of continuum magnetomechanics. We then go on to describe a thermodynamically consistent constitutive theory and proceed to show, how we can solve such coupled boundary value problems, within in a variational framework.

The fourth chapter, presents an alternative compact finite element formulation used to solve the boundary value problems. This is the formulation that has been used in

obtaining the numerical results that have been presented in the penultimate section of the thesis.

The fifth chapter, gives the details of the material models used for the numerical implementation i.e. the free energy function and the resulting constitutive equations. These models have been implemented in a finite element framework to obtain the results reported in the following section.

The sixth chapter reports the numerical results. In order to test the response of the material models at the material point level, we have described two driver algorithms to do the same.

The seventh chapter concludes the thesis with an outline of what has been achieved in the present work and brief outlook for possible further research in the field.

2. Motivation: Macroscopic Response of MRE

The magneto-sensitive materials described in the previous section may be either *isotropic* or *anisotropic* which depends on the method of preparation. Magnetoelasts are prepared by dispersing nano or micro sized iron particles in the rubber during the curing process. This may be done in the presence or absence of a magnetic field. If there is no magnetic field present, we get isotropic distribution of iron particles in the matrix whereas if there is a magnetic field present, we have the iron particles aligned along the applied magnetic field which gives a preferred direction or *transverse anisotropy*.

Figure 1 is a Scanning Electron Microscope (SEM) picture of iron particles in silicone M4601 matrix which shows the microstructure of the two types of isotropy.

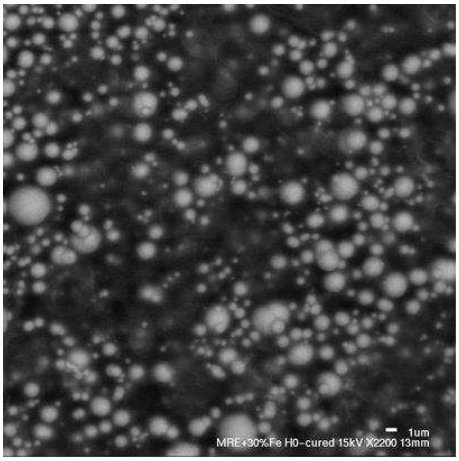

(a) Isotropic or random distribution of iron particles in matrix.

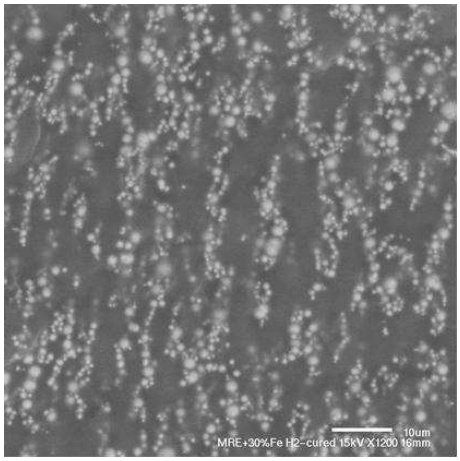

(b) Iron particles aligned in a preferred direction.

Figure 1: SEM pictures of microstructure of MRE- Iron particles in silicone M4601 matrix. Reference: Kallio [18]

Figure 2 consequently, is a schematic representation of the microstructures described above along with possible loading directions for compressions. It also shows that while two different experiments are required to determine the elastic modulus of isotropic magnetic elastomers, five would be required for the transversely anisotropic counterpart.

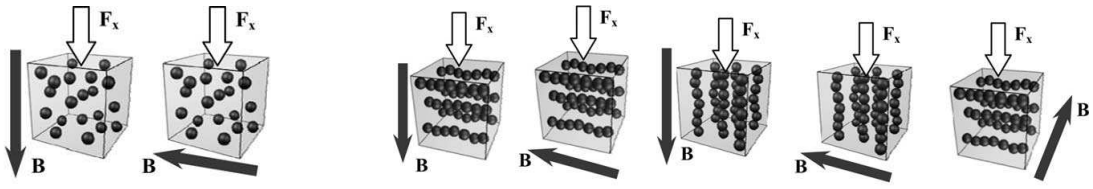

(a) Isotropic

(b) Anisotropic

Figure 2: Schematic of microstructures Reference: Varga, Filipcsei & Zrínyi [2005]

In what follows, an overview of the experimental data available is presented which, along with the knowledge of microstructure, is used as motivation for the development of the constitutive models i.e. the *free-energy functions* presented in the next chapter.

2.1. Isotropic Magnetorheological Elastomers

Here the iron particles are randomly distributed in the matrix. Experimental results from JOLLY ET. AL [17] for a double lap shear specimen using a Dynastat ® material testing system are shown in Figure 3(a). This system applies a fixed oscillatory strain to the specimen and measures the amplitude and phase of the output from which the shear modulus may be calculated. Magnetic fields were applied to the test specimen using the horseshoe shaped electromagnet with poles that efficiently focus magnetic flux across the elastomer segments in the direction shown in Figure 3.

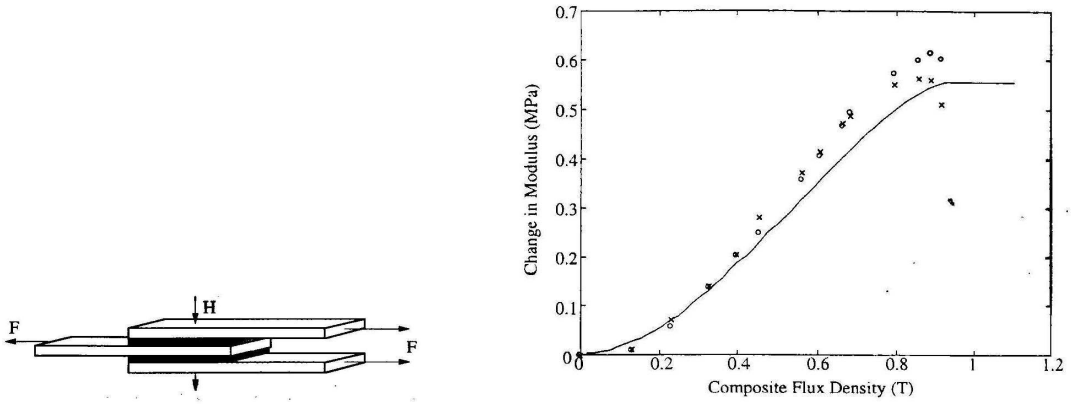

(a) Experimental setup (b) Change in modulus modulus vs applied $\boldsymbol{H}$

Figure 3: Shear test on isotropic specimen. Reference: JOLLY ET AL. [1996].

The results of the experiment show that the shear modulus increases with magnetic field until it reaches a saturation value. A consistent explanation for this effect may be given by looking at the microstructure of such materials. Since the iron particles in the within the matrix have a saturation value of magnetization, the same should be observed with the shear modulus since the magnetization determines the magnitude of the interparticle forces of attraction.

Figure 4 shows the stress-strain plot for a sample that contains random distribution of iron particles within the matrix of the elastomer. It shows that the response is indeed close to a Neo-Hookean response and motivates us to use a Neo-Hookean type free energy function to model these kinds of materials. However we must modify the Neo-Hookean free energy to include the stiffening effect of the magnetic field on the material.

The main features to be accounted for, are summarized below.

- *Feature 1:* Response in a constant magnetic field should be Neo-Hookean as indicated by Figure 4.

- *Feature 2:* With increasing magnetic field, the material should have a stiffer response ie. higher shear modulus, due to increased interparticle magnetic attraction.

- *Feature 3:* The shear modulus should saturated with increasing magnetic field strength.

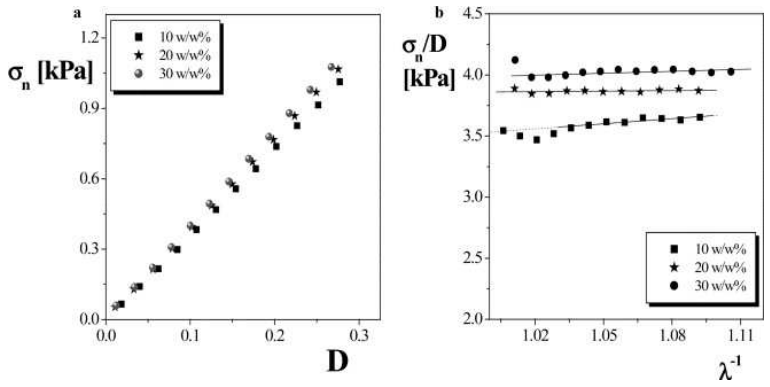

Figure 4: Stress vs. Strain measurements for Poly (dimethyl siloxane) sample Reference: Varga, Filipcsei & Zrínyi [2005]. Here $\mathbf{D} = \lambda - \lambda^{-2}$ where λ is the *stretch*.

2.2. Magnetorheological Elastomers with Transverse-Anisotropy

As mentioned earlier, if a magnetic field is applied during the curing process of the MRE, then the iron particles get aligned along along a *preferred direction* leading to transversely isotropic microstructure as shown in Figure 1.

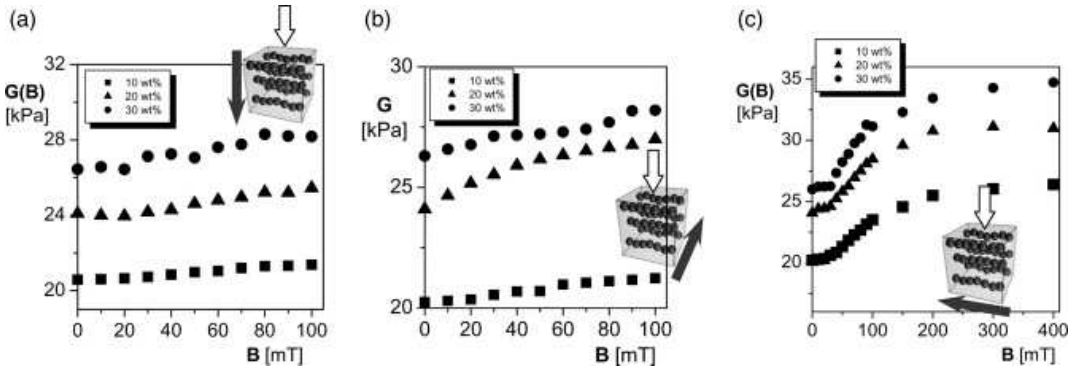

Figure 5: Effect of the magnetic field intensity on the elastic modulus for transversely isotropic samples of magnetoelasts containing different amount of carbonyl-iron particles. Here the mechanical loading is perpendicular to chains while magnetic field assumes different directions. Reference: Varga, Filipcsei & Zrínyi [2005].

Figure 5 and Figure 6 show that the shear modulus G is hardly changed when a magnetic field is applied perpendicular to the direction of the chains. When they are parallel however, the coupling is 'switched on' and the shear modulus changes significantly with magnetic field.

Thus, we state the features to be captured by a *transversely isotropic* model as follows.

- *Feature 1:* When the magnetic field is perpendicular to the chain direction, response is unaffected by magnetic field strength.
- *Feature 2:* When the magnetic field is parallel to the chains, the shear modulus increases.
- *Feature 3:* One might expect buckling at high compressive strains due to the columnar arrangement of iron particles.

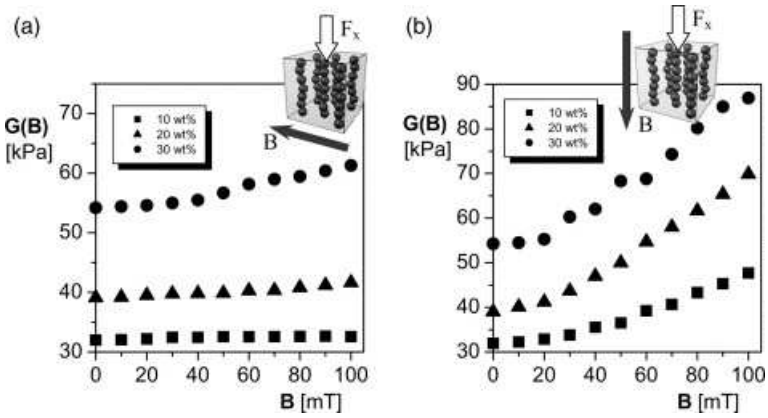

Figure 6: Effect of the magnetic field intensity on the elastic modulus for transversely isotropic magnetoelasts containing different abount of carbonyl-iron particles. Reference: Varga, Filipcsei & Zrínyi [2005]. In both cases compression is in the direction of the chains but magnetic field has different directions.

2.3. Importance of Boundary Conditions

Apart from the expected characteristics of material models another important consideration is the application of magnetic boundary conditions. Figure 7 shows a typical experimental setup for conducting thermo-magneto-mechanical experiments (cf. [20]). One may observe that the magnetic boundary conditions are not applied on the boundary of the specimen but rather in the free-space adjoining it. This is because, a magnetic potential difference $\Delta\Phi$ is applied with the help of a current carrying coil and this is usually placed at some distance from the sample.

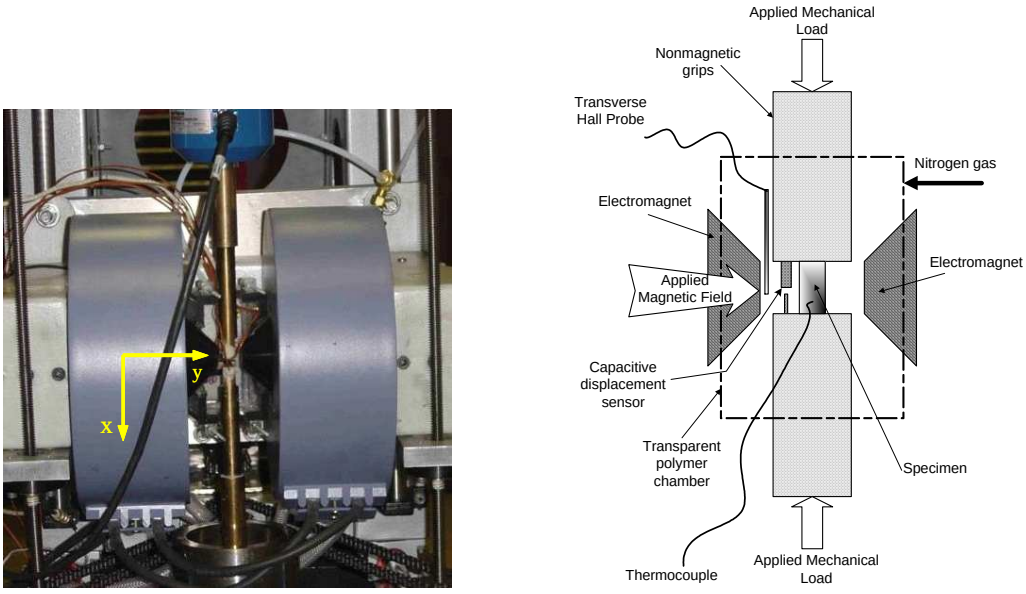

(a) Actual experimental setup (b) Schematic of experimental setup

Figure 7: Experimental setup in [20] for thermo-magneto-mechanical experiments.

This may be contrasted with the corresponding *electric case* where we may have *electro-active materials* that are subjected to the equivalent *electric boundary conditions*.

Here, the *electric potential*, is applied with the help of electrodes (cathode-anode), which may be painted to the surface. However, in the magnetic case, we do not have a magnetic equivalent of an electrode (since magnetic monopoles have not been found to exist). Therefore the closest we can get to applying the magnetic potential directly on the surface, is by having a closed circuit with zero air gap. To have no air gap, one may need to apply some pressure on the sample with the two ends. Enforcing this zero air gap is thus, not only impractical but also interferes with the deformation of the sample as can be seen in Figure 8.

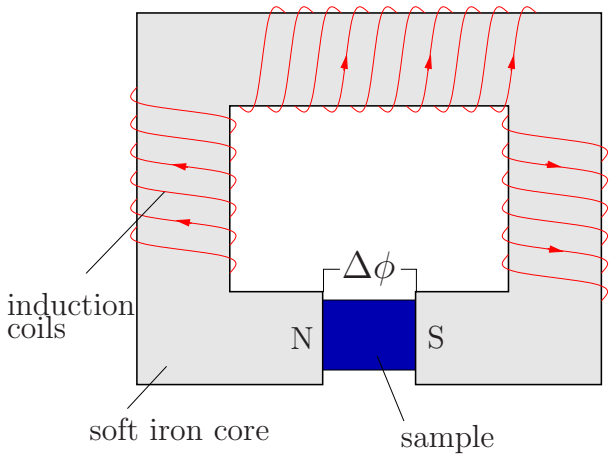

Figure 8: The magnetic circuit shown in the sketch may be considered *closed*, if the air gaps between the magnetic material sample and the iron core are negligible. Such an experimental setup may be considered the best physical approximation of magnetic potential boundary conditions prescribed at the sample surface.

This motivates us to include the adjoining free space in our boundary value problems with the boundary conditions being applied on the surface of this free-space rather than directly on the surface of the body.

3. Introduction to Continuum Magnetomechanics at Finite Strains

In this chapter the continuum-thermodynamics basis for a finite deformation theory with an extension to magnetostatics is established. This derivation includes the typical steps of defining the finite deformation kinematics based on fundamental geometric mappings, of introducing stress measures, the basic magnetic field variables as well as the global and local balance laws of continuum magnetomechanics.

The following description of finite deformation kinematics conceptually relies on the terminology of modern differential geometry (cf. MARSDEN & HUGHES [24]).

3.1. Geometrical Aspects of Finite Deformation Kinematics

A *material body* B is mathematically defined as the open set of material points P, which can be identified with geometrical points in the three-dimensional Euclidean space $\mathbb{R}^3$ via the one-to-one *configuration placement map* $\boldsymbol{\chi}$. The *motion* of a body is the time-parameterized family of configurations

$$\boldsymbol{\chi}_t := \begin{cases} B \to \mathcal{B}_t \in \mathbb{R}^3 \ , \\ P \in B \mapsto \boldsymbol{x}_t = \boldsymbol{\chi}_t(P) \in \mathcal{B}_t \ . \end{cases} \tag{1}$$

This relation therefore describes the configuration of the body B in $\mathbb{R}^3$ at time t. In the *referential description of motion* one defines the *reference* or *Lagrangian configuration* as the placement of the body at time t_0, i.e. $\mathcal{B} := \boldsymbol{\chi}_{t_0}(B)$, with the *reference coordinates* $\boldsymbol{X} := \boldsymbol{\chi}_{t_0}(P) \in \mathcal{B}$. The *current* or *Eulerian configuration* at time t is defined as $\mathcal{S} := \boldsymbol{\chi}_t(B)$, with the *spatial coordinates* $\boldsymbol{x} := \boldsymbol{\chi}_t(P) \in \mathcal{S}$. The motion of the body with respect to the

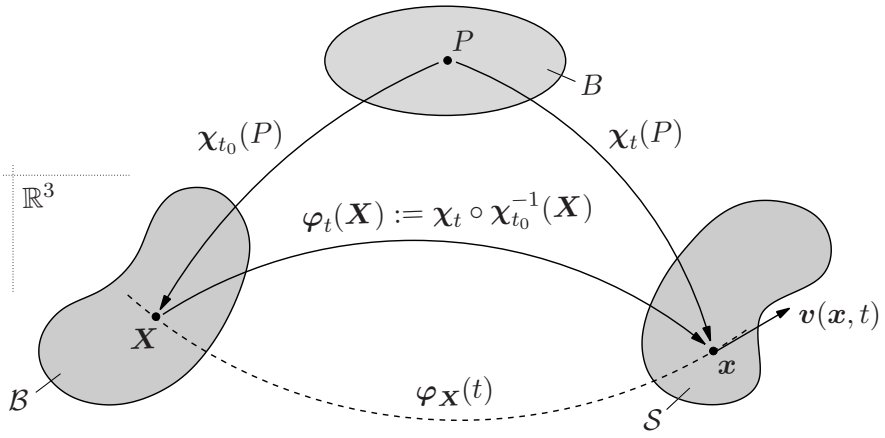

Figure 9: Identification of the position $\boldsymbol{X} \in \mathcal{B}$ of a particle $\boldsymbol{P} \in B$ in three-dimensional Euclidian space $\mathbb{R}^3$ through the configuration map $\boldsymbol{\chi}_t$ and description of the motion of a material point w.r.t the reference configuration via the deformation map $\boldsymbol{\varphi}_t$.

reference configuration is then defined by the nonlinear *deformation map*

$$\boldsymbol{\varphi} := \begin{cases} \mathcal{B} \times \mathbb{R}_+ \to \mathcal{S} \in \mathbb{R}^3 \ , \\ (\boldsymbol{X}, t) \mapsto \boldsymbol{x} = \boldsymbol{\varphi}(\boldsymbol{X}, t) = \boldsymbol{\varphi}_t(\boldsymbol{X}) \ , \end{cases} \tag{2}$$

which maps the material points $\boldsymbol{X} \in \mathcal{B}$ onto their deformed spatial positions $\boldsymbol{x} \in \mathcal{S}$ as shown in Figure 9.

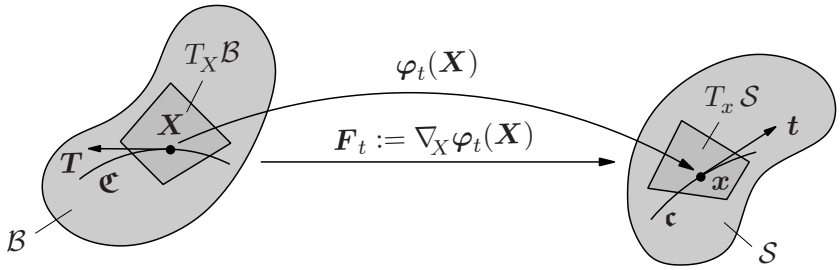

Figure 10: The deformation gradient acting as the linear tangent map, which transforms the material vector $\boldsymbol{T} \in T_X\mathcal{B}$, tangent to a material curve $\mathfrak{C}$ at $\boldsymbol{X}$, onto the associated spatial vector $\boldsymbol{t} \in T_x\,\mathcal{S}$, tangent to the material curve $\mathfrak{c}$ at $\boldsymbol{x}$.

Mathematically, the *deformation gradient* $\boldsymbol{F}$ is defined as the Fréchet derivative of the deformation map, i.e. $\boldsymbol{F}_t(\boldsymbol{X}) := \operatorname{Grad} \boldsymbol{\varphi}_t$. Geometrically, the deformation gradient can be interpreted as the *linear tangent map* which maps tangents $\boldsymbol{T}$ to material curves, i.e. elements of the tangent spaces $T_X\mathcal{B}$ of the manifold $\mathcal{B}$, onto tangents $\boldsymbol{t}$ of the deformed material curves, i.e. elements of the tangent space $T_x\,\mathcal{S}$ of the manifold $\mathcal{S}$, according to

$$\boldsymbol{F}_t := \begin{cases} T_X\mathcal{B} \to T_x\,\mathcal{S} \ , \\ \boldsymbol{T} \mapsto \boldsymbol{t} = \boldsymbol{F}_t\boldsymbol{T} \ , \end{cases} \tag{3}$$

as visualized in Figure 10. Note that, since $\boldsymbol{\varphi}_t$ is a one-to-one mapping and must prohibit material interpenetration, the deformation gradient is subject to the following constraints $J := \det \boldsymbol{F} > 0$. The determinant of the deformation gradient can further directly be interpreted as another fundamental mapping, the *volume map*, which relates infinitesimal reference volume elements dv to their deformed spatial counterparts dV via the relation

$$J = \det \boldsymbol{F} := \begin{cases} \mathbb{R}_+ \to \mathbb{R}_+ \ , \\ dV \mapsto dv = \det \boldsymbol{F}\, dV \ . \end{cases} \tag{4}$$

The *co-factor* of the deformation gradient $\operatorname{cof} \boldsymbol{F}$ is defined as the derivative of the volume map with respect to $\boldsymbol{F}$. It can geometrically be interpreted as the *area map*, which maps infinitesimal reference area elements onto the associated spatial ones via the relation $\boldsymbol{n}\, da = J\boldsymbol{F}^{-T}\boldsymbol{N}\, dA = (\operatorname{cof} \boldsymbol{F})\boldsymbol{N}\, dA$, also known as *Nanson's formula*. Moreover, $\boldsymbol{F}^{-T}$ can thus be identified as the *normal map*, that maps normals of material surfaces, or, again from the differential geometry view point, elements of the co-tangent space $T_X^*\mathcal{B}$, onto normals of the deformed spatial surfaces, i.e. elements of the co-tangent space $T_x^*\mathcal{S}$, according to

$$\boldsymbol{F}^{-T} := \begin{cases} T_X^*\mathcal{B} \to T_x^*\mathcal{S} \ , \\ \boldsymbol{N} \mapsto \boldsymbol{n} = \boldsymbol{F}^{-T}\boldsymbol{N} \ . \end{cases} \tag{5}$$

For the specification of coordinate representations one introduces the Cartesian frames $\{\boldsymbol{E}_i\}$ for $T_X\mathcal{B}$, $\{\boldsymbol{E}^i\}$ for $T_X^*\mathcal{B}$, $\{\boldsymbol{e}_i\}$ for $T_x\,\mathcal{S}$ and $\{\boldsymbol{e}^i\}$ for $T_x^*\mathcal{S}$. Capital letter indices $i = \{A, B, C\}$ are used for Lagrangian and lower case indices $i = \{a, b, c\}$ for Eulerian settings.[1] The reference and spatial coordinates are thus expressed as $\boldsymbol{X} = X^A\boldsymbol{E}_A$ and

[1]Note that these frames will typically coincide, but they have formally been considered here for the sake of clarity.

$\boldsymbol{x} = x^a \boldsymbol{e}_a$. The deformation gradient then admits the representation $\boldsymbol{F} = F^a{}_A \boldsymbol{e}_a \otimes \boldsymbol{E}^A$, with $F^a{}_A = \partial\varphi^a/\partial X^A$. Likewise, the component forms of the mappings (3) and (5) read $t^a = F^a{}_A T^A$ and $n_a = (F^{-1})^A{}_a N_A$.

In order to be able to measure geometric quantities such as the length of vectors, however, one must additionally introduce *metric tensors*. In global Cartesian frames the *covariant* and *contravariant Lagrangian metric tensors* admit the reduced representation $\boldsymbol{G} = \delta_{AB}\boldsymbol{E}^A \otimes \boldsymbol{E}^B$ and $\boldsymbol{G}^{-1} = \delta^{AB}\boldsymbol{E}_A \otimes \boldsymbol{E}_B$, where δ_{AB} and δ^{AB} are Kronecker deltas. Similarly, the *covariant* and *contravariant Eulerian metric tensors* reduce to $\boldsymbol{g} = \delta_{ab}\boldsymbol{e}^a \otimes \boldsymbol{e}^b$ and $\boldsymbol{g}^{-1} = \delta^{ab}\boldsymbol{e}_a \otimes \boldsymbol{e}_b$, respectively. The metric tensors represent mappings of vectors, i.e. elements of the tangent spaces, onto normals (co-vectors), i.e. elements of the co-tangent spaces. For the Lagrangian and the Eulerian manifolds these mappings are defined by

$$\boldsymbol{G} := \begin{cases} T_X\mathcal{B} \to T_X^*\mathcal{B} \ , \\ \boldsymbol{T} \mapsto \boldsymbol{N} = \boldsymbol{G}\boldsymbol{T} \ , \end{cases} \qquad \boldsymbol{g} := \begin{cases} T_x\,\mathcal{S} \to T_x^*\mathcal{S} \ , \\ \boldsymbol{t} \mapsto \boldsymbol{n} = \boldsymbol{g}\boldsymbol{t} \ . \end{cases} \tag{6}$$

These mappings can also be interpreted as *index lowering* or *raising procedures* since the coordinate representations of (6) read $N_A = G_{AB}T^B = \delta_{AB}T^B$ and $n_a = g_{ab}t^b = \delta_{ab}t^b$, respectively. It is

Commutative diagrams, such as the ones displayed in Figure 11, significantly facilitate the geometric meaning of the introduced mappings. Based on the definitions of the

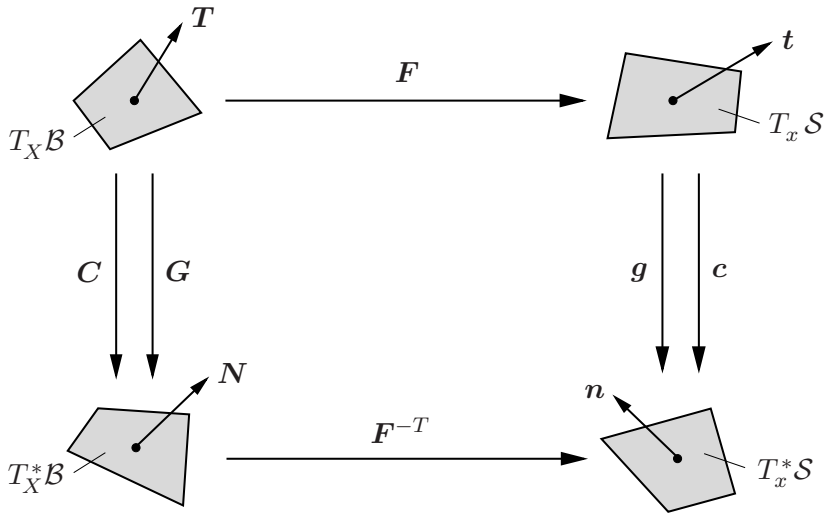

Figure 11: Commutative diagram illustrating the *'push-forward'* and *'pull-back'* of the covariant reference metric $\boldsymbol{G}$ and spatial metric $\boldsymbol{g}$.

mappings (3), (5), (6) and their respective inverse mappings, one can introduce additional deformation measures. The *right Cauchy-Green tensor* $\boldsymbol{C}$ can in this context be defined as the *'pull-back'* of the spatial metric

$$\boldsymbol{C} := \boldsymbol{\varphi}^*(\boldsymbol{g}) = \boldsymbol{F}^T\boldsymbol{g}\boldsymbol{F} \ , \qquad \text{or} \qquad C_{AB} = F^a{}_A g_{ab} F^b{}_B \ , \tag{7}$$

in coordinate representation, and can thus be interpreted as the 'representation of the current metric in the Lagrangian setting' or 'convected spatial metric'. Similarly, the *inverse right Cauchy-Green tensor* $\boldsymbol{C}^{-1}$ is defined as

$$\boldsymbol{C}^{-1} := \boldsymbol{\varphi}^*(\boldsymbol{g}^{-1}) = \boldsymbol{F}^{-1}\boldsymbol{g}^{-1}\boldsymbol{F}^{-T} \ , \qquad \text{or} \qquad \big(C^{-1}\big)^{AB} = \big(F^{-1}\big)^A{}_a g^{ab} \big(F^{-1}\big)^B{}_b \ . \tag{8}$$

Accordingly, via appropriate *'push-forward'* operations, one defines the *left Cauchy-Green tensor* $\boldsymbol{b}^f$, often called the *Finger tensor*, and the *inverse left Cauchy-Green tensor* $\boldsymbol{c}$, respectively, as

$$\boldsymbol{b}^f := \boldsymbol{\varphi}_* \left(\boldsymbol{G}^{-1}\right) = \boldsymbol{F}\boldsymbol{G}^{-1}\boldsymbol{F}^T \ , \qquad \text{or} \qquad b^{ab} = F^a{}_A G^{AB} F^b{}_B \ , \tag{9}$$

$$\boldsymbol{c} = \left(\boldsymbol{b}^f\right)^{-1} := \boldsymbol{\varphi}_* \left(\boldsymbol{G}\right) = \boldsymbol{F}^{-T}\boldsymbol{G}\boldsymbol{F}^{-1} \ , \qquad \text{or} \qquad c_{ab} = \left(F^{-1}\right)^A{}_a G_{AB} \left(F^{-1}\right)^B{}_b \ . \tag{10}$$

The reader is again referred to Figure 11 for a graphical representation of the geometrical mapping properties of the introduced metric tensors.

3.2. Fundamental Stress Measures

Consider an arbitrary *part* $\mathcal{P} \subset \mathcal{B}$ cut out of the undeformed body in the reference configuration and its deformed counterpart $\mathcal{P}_t \subset \mathcal{S}$ with the respective closed surfaces $\partial\mathcal{P}$ and $\partial\mathcal{P}_t$, as shown in Figure 12. In the current configuration one replaces the mechanical action of the rest of the body on the cut-out part by the spatial traction field $\boldsymbol{t}$. According

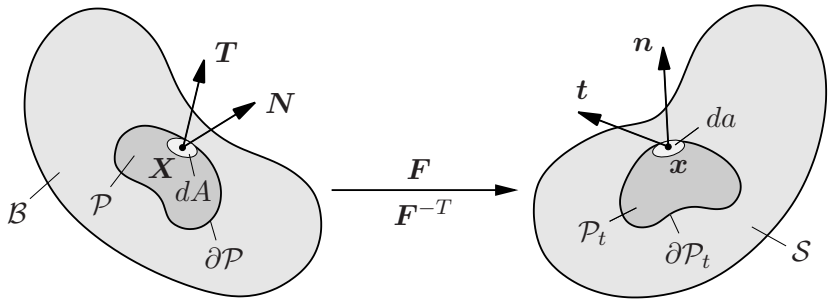

Figure 12: The material and spatial traction vectors $\boldsymbol{T}(\boldsymbol{X}, t; \boldsymbol{N}) \in T_X\mathcal{B}$ and $\boldsymbol{t}(\boldsymbol{x}, t; \boldsymbol{n}) \in T_x\mathcal{S}$ representing the forces per unit area exerted by the cut-off remainder of the body on the surfaces $\partial\mathcal{P}$ and $\partial\mathcal{P}_t$ of the cut-out parts in the material and spatial settings, respectively.

to *Cauchy's theorem*, $\boldsymbol{t}$ is assumed to be a linear function of the orientation of the cut, represented by the spatial unit normal $\boldsymbol{n} \in T_x^*\mathcal{S}$ to the surface $\partial\mathcal{P}_t$, or specifically

$$\boldsymbol{t}(\boldsymbol{x}, t; \boldsymbol{n}) := \boldsymbol{\sigma}(\boldsymbol{x}, t)\boldsymbol{n} \ , \qquad \text{or} \qquad t^a = \sigma^{ab} n_b \ . \tag{11}$$

Therein $\boldsymbol{\sigma}$ is the *Cauchy stress tensor*, which in our considered geometrical framework can be understood as a contravariant mapping of the form

$$\boldsymbol{\sigma} := \begin{cases} T_x^*\mathcal{S} \to T_x\mathcal{S} \ , \\ \boldsymbol{n} \mapsto \boldsymbol{t} = \boldsymbol{\sigma}\boldsymbol{n} \ . \end{cases} \tag{12}$$

Another common spatial stress measure is the *Kirchhoff stress tensor*, or *weighted Cauchy stress tensor*, $\boldsymbol{\tau} := J\boldsymbol{\sigma}$, which, due to the scalar nature of J, preserves the geometric mapping properties of $\boldsymbol{\sigma}$.

One can further introduce a scaled spatial traction vector $\tilde{\boldsymbol{t}} \in T_x\mathcal{S}$ that produces a resultant force on an element of the reference surface which is equal to the force exerted by $\boldsymbol{t}$ on an element of the deformed surface, such that $\boldsymbol{t}\, da = \tilde{\boldsymbol{t}}\, dA$. The *nominal* or *first Piola-Kirchhoff stress tensor* $\boldsymbol{P}$ is then defined via the Cauchy-theorem-type relation

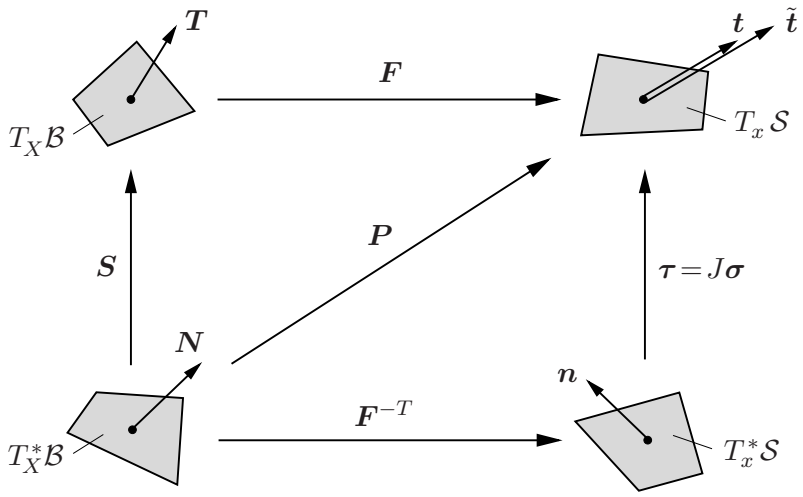

Figure 13: Commutative diagram illustrating the geometric mapping properties of the introduced stress tensors.

$\tilde{\boldsymbol{t}} := \boldsymbol{P}\boldsymbol{N}$, or $\tilde{t}^a = P^{aA}N_A$. Additionally, using Nanson's formula, one obtains the following relation between the introduced stress tensors $\boldsymbol{P} = J\boldsymbol{\sigma}\boldsymbol{F}^{-T} = \boldsymbol{\tau}\boldsymbol{F}^{-T}$. Note that $\boldsymbol{P}$ is a two-point (mixed-variant) tensor possessing the geometrical mapping properties

$$\boldsymbol{P} := \begin{cases} T^*_X\mathcal{B} \to T_x\,\mathcal{S}\ , \\ \boldsymbol{N} \mapsto \tilde{\boldsymbol{t}} = \boldsymbol{P}\boldsymbol{N}\ . \end{cases} \tag{13}$$

The Lagrangian traction vector $\boldsymbol{T} \in T_X\mathcal{B}$ may be defined as the *'pull-back'* of the spatial traction field $\tilde{\boldsymbol{t}} \in T_x\,\mathcal{S}$, i.e. $\boldsymbol{T} = \boldsymbol{\varphi}^*\left(\tilde{\boldsymbol{t}}\right) = \boldsymbol{F}^{-1}\boldsymbol{T}$ as displayed in Figure 12. The *second Piola-Kirchhoff stress tensor* $\boldsymbol{S}$ is then defined via the relation $\boldsymbol{T} := \boldsymbol{S}\boldsymbol{N}$, or $T^A = S^{AB}N_B$, and has the mapping properties

$$\boldsymbol{S} := \begin{cases} T^*_X\mathcal{B} \to T_X\mathcal{B}\ , \\ \boldsymbol{N} \mapsto \boldsymbol{T} = \boldsymbol{S}\boldsymbol{N}\ . \end{cases} \tag{14}$$

The commutative diagram of Figure 13 depicts the geometrical relations between the introduced stress tensors. It is immediately apparent that the following *'pull-back'* operations on the mixed-variant and spatial stress tensors hold.

$$\boldsymbol{S} := \boldsymbol{\varphi}^*(\boldsymbol{P}) = \boldsymbol{F}^{-1}\boldsymbol{P}\ , \qquad \text{or} \qquad S^{AB} = \left(F^{-1}\right)^A{}_a P^{aB}\ , \tag{15}$$

$$\boldsymbol{S} := \boldsymbol{\varphi}^*(\boldsymbol{\tau}) = \boldsymbol{F}^{-1}\boldsymbol{\tau}\boldsymbol{F}^{-T}\ , \qquad \text{or} \qquad S^{AB} = \left(F^{-1}\right)^A{}_a \tau^{ab}\left(F^{-1}\right)^B{}_b\ . \tag{16}$$

Accordingly, the converse *'push-forward'* relations of the mixed-variant and reference stress tensors are given by

$$\boldsymbol{\tau} = J\boldsymbol{\sigma} := \boldsymbol{\varphi}_*(\boldsymbol{P}) = \boldsymbol{P}\boldsymbol{F}^T\ , \qquad \text{or} \qquad \tau^{ab} = P^{aA}F^b{}_A\ , \tag{17}$$

$$\boldsymbol{\tau} := \boldsymbol{\varphi}_*(\boldsymbol{S}) = \boldsymbol{F}\boldsymbol{S}\boldsymbol{F}^T\ , \qquad \text{or} \qquad \tau^{ab} = F^a{}_A S^{AB} F^b{}_B\ . \tag{18}$$

3.3. Balance Principles of Continuum Thermo-Magneto-Mechanics

In this section the balance principles of continuum thermomechanics are briefly reviewed and the main focus is placed on their extension to the continuum mechanics of

magnetizable matter. This step requires the addition of terms in the thermomechanical balance laws, as well as the introduction of Maxwell's equations. Extensive discussions of the *electrodynamics of continua* have been presented by Pao & Hutter [27], Pao [26], Hutter & van de Ven [15], Maugin [25], Eringen and Maugin [13].

3.3.1. Maxwell's Equations of Continuum Electrodynamics. The electrodynamics of polarizable and magnetizable moving continua are in the non-relativistic limit described by the following *global form* of Maxwell's equations

$$\text{Gauss' law} \qquad \int_{\partial\mathcal{P}_t} \boldsymbol{d}\cdot\boldsymbol{n}\,da = \int_{\mathcal{P}_t} \rho_f\,dv\ , \tag{19a}$$

$$\text{Gauss-Faraday law} \qquad \int_{\partial\mathcal{P}_t} \boldsymbol{b}\cdot\boldsymbol{n}\,da = 0\ , \tag{19b}$$

$$\text{Faraday's law} \qquad \int_{\partial\mathcal{A}_t} \boldsymbol{e}'\cdot\,d\boldsymbol{x} = -\frac{d}{dt}\int_{\mathcal{A}_t} \boldsymbol{b}\cdot\boldsymbol{n}\,da\ , \tag{19c}$$

$$\text{Ampère's law} \qquad \int_{\partial\mathcal{A}_t} \boldsymbol{h}'\cdot\,d\boldsymbol{x} = \int_{\mathcal{A}_t} \boldsymbol{j}'_f\cdot\boldsymbol{n}\,da + \frac{d}{dt}\int_{\mathcal{A}_t} \boldsymbol{d}\cdot\boldsymbol{n}\,da\ , \tag{19d}$$

where $\boldsymbol{e}$ is the *electric field strength*, $\boldsymbol{d}$ the *dielectric displacement*, ρ_f the *electric charge density* and $\boldsymbol{j}_f$ the *free current density*. Primed field variables indicate that they are measured with respect to the *rest-frame*, or in other words a co-moving observer.[2] The above integrations in the spatial setting are carried out either over the part $\mathcal{P}_t\subset\mathcal{S}$ and its boundary $\partial\mathcal{P}_t$ or an arbitrary material surface $\mathcal{A}_t$ with boundary $\partial\mathcal{A}_t$. Note further that by applying Ampère's law to a closed surface, such that $\mathcal{A}_t=\partial\mathcal{P}_t$ and $\partial\mathcal{A}_t=\emptyset$, and using Gauss' law one obtains the expression

$$\frac{d}{dt}\int_{\mathcal{P}_t} \rho_f\,dv + \int_{\partial\mathcal{P}_t} \boldsymbol{j}'_f\cdot\boldsymbol{n}\,da = 0\ , \tag{20}$$

commonly known as the *conservation of charge* equation.[3]

By applying the divergence theorem, Stokes' theorem and the following transport theorem for the rate of change of the flux of a spatial vector field $\boldsymbol{\psi}$ through the material

[2]The transformation relations of the rest frame variables to the variables measured with respect to the *laboratory frame*, i.e. with respect to a stationary observer, depend on the basic invariance properties of the chosen formulation (cf. [15]). As an example, the field transformation relations of the *Minkowski formulation* are given by $\boldsymbol{e}'=\boldsymbol{e}+\boldsymbol{v}\times\boldsymbol{b}$, $\boldsymbol{h}'=\boldsymbol{h}-\boldsymbol{v}\times\boldsymbol{d}$ and $\boldsymbol{j}'_f=\boldsymbol{j}_f-\rho_f\boldsymbol{v}$.

[3]Different standpoints have been expressed in the literature on which of Maxwell's equations are of fundamental nature and whether they can be considered *conservation laws*. Hutter and van de Ven for example argue that Faraday's law, often also referred to as the *conservation of magnetic flux*, and the conservation of charge equations should be considered the two fundamental conservation laws. The Gauss-Faraday law would then be considered a special case of the former for closed surfaces and further Gauss' law and Ampère's law simply as *definitions* of the dielectric displacement field and the magnetic field, respectively. Other authors, however, disagree with this concept and consider all four Maxwell equations as basic and the conservation of charge equation as a consistent consequence.

surface $\mathcal{A}_t$

$$\frac{d}{dt}\int\limits_{\mathcal{A}_t} \boldsymbol{\psi}\cdot\boldsymbol{n}\,da = \int\limits_{\mathcal{A}_t} \overset{\star}{\boldsymbol{\psi}}\cdot\boldsymbol{n}\,da = \int\limits_{\mathcal{A}_t}\left[\frac{\partial\boldsymbol{\psi}}{\partial t} + \boldsymbol{v}\,\mathrm{div}\,\boldsymbol{\psi} - \mathrm{curl}\,(\boldsymbol{v}\times\boldsymbol{\psi})\right]\cdot\boldsymbol{n}\,da\ , \tag{21}$$

to the global form of Maxwell's equations (19) and then localizing, one can derive the *local form* of Maxwell's equations for electromagnetic continua

$$\text{Gauss' law} \qquad \mathrm{div}\,\boldsymbol{d} = \rho_f\ , \tag{22a}$$

$$\text{Gauss-Faraday law} \qquad \mathrm{div}\,\boldsymbol{b} = 0\ , \tag{22b}$$

$$\text{Faraday's law} \qquad \mathrm{curl}\,\boldsymbol{e}' = -\overset{\star}{\boldsymbol{b}}\ , \tag{22c}$$

$$\text{Ampère's law} \qquad \mathrm{curl}\,\boldsymbol{h}' = \boldsymbol{j}'_f + \overset{\star}{\boldsymbol{d}}\ , \tag{22d}$$

If, in particular, we restrict our attention to charge-free, non-polarizable media and consider the slow-speed approximation of *magnetostatics*, then electric effects may be neglected and no distinction is made between moving and stationary frames. The now *decoupled Maxwell equations of magnetostatics* are then given by the following global and local expressions

$$\text{Gauss-Faraday law} \quad \int\limits_{\partial\mathcal{P}_t}\boldsymbol{b}\cdot\boldsymbol{n}\,da = 0\ , \qquad \mathrm{div}\,\boldsymbol{b} = 0\ , \tag{23a}$$

$$\text{Ampère's law} \quad \int\limits_{\partial\mathcal{A}_t}\boldsymbol{h}\cdot\,d\boldsymbol{x} = \int\limits_{\mathcal{A}_t}\boldsymbol{j}_f\cdot\boldsymbol{n}\,da\ , \qquad \mathrm{curl}\,\boldsymbol{h} = \boldsymbol{j}_f\ . \tag{23b}$$

Using the geometrical framework of finite kinematics introduced in Section 3.1, one can proceed to derive the material description of Maxwell's equations. Using the area map it follows

$$\int\limits_{\partial\mathcal{P}_t}\boldsymbol{b}\cdot\boldsymbol{n}\,da = \int\limits_{\partial\mathcal{P}}\boldsymbol{b}\cdot J\boldsymbol{F}^{-T}\boldsymbol{N}\,dA = \int\limits_{\partial\mathcal{P}}\boldsymbol{B}\cdot\boldsymbol{N}\,dA\ , \tag{24}$$

where we have defined the *reference magnetic induction field* via the relation $\boldsymbol{B} := J\boldsymbol{F}^{-1}\boldsymbol{b}$, or $B^A = J(F^{-1})^A{}_a b^a$. Analogously, the free current density transforms according to the relation $\boldsymbol{J}_f := J\boldsymbol{F}^{-1}\boldsymbol{j}_f$. Using the mapping properties of the deformation gradient, it also follows

$$\int\limits_{\partial\mathcal{A}_t}\boldsymbol{h}\cdot\,d\boldsymbol{x} = \int\limits_{\partial\mathcal{A}}\boldsymbol{h}\cdot\boldsymbol{F}\,d\boldsymbol{X} = \int\limits_{\partial\mathcal{A}}\boldsymbol{H}\cdot\,d\boldsymbol{X}\ , \tag{25}$$

with the definition of the *reference magnetic field strength* $\boldsymbol{H} := \boldsymbol{F}^T\boldsymbol{h}$, or $H_A = F^a{}_A h_a$. The derived geometric relations are again visualized in a commutative diagram shown in Figure 14. Based on the above derivations one obtains the *Maxwell equations of magnetostatics in the Lagrangian setting* in global and local form

$$\text{Gauss-Faraday law} \quad \int\limits_{\partial\mathcal{P}}\boldsymbol{B}\cdot\boldsymbol{N}\,dA = 0\ , \qquad \mathrm{Div}\,\boldsymbol{B} = 0\ , \tag{26a}$$

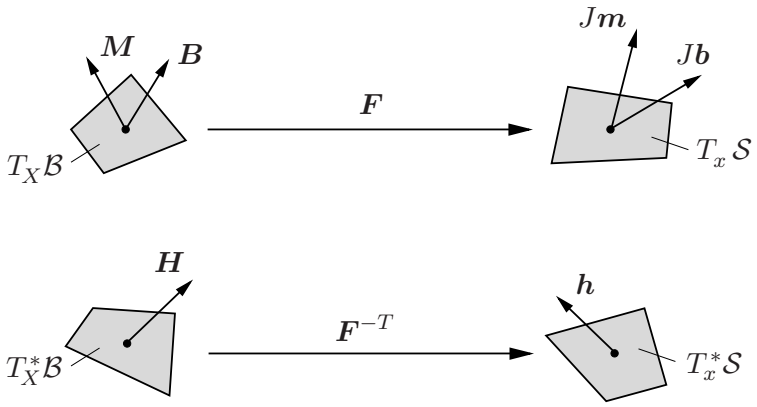

Figure 14: Commutative diagram illustrating the geometric mapping relations between material and spatial magnetic field variables.

$$\text{Ampère's law} \qquad \int_{\partial\mathcal{A}} \boldsymbol{H} \cdot d\boldsymbol{X} = \int_{\mathcal{A}} \boldsymbol{J}_f \cdot \boldsymbol{N}\, dA\ , \qquad \text{Curl}\, \boldsymbol{H} = \boldsymbol{J}_f\ . \tag{26b}$$

In free space (vacuum) the magnetic induction and the magnetic field are related by the expression $\boldsymbol{b} = \mu_0 \boldsymbol{g}^{-1}\boldsymbol{h}$. In matter it is often convenient to introduce an additional variable, the *spatial magnetization field* $\boldsymbol{m}$, which represents the contribution to the overall magnetic induction caused by the interaction of the magnetic field with the magnetized material. One thus obtains the general constitutive-type relation

$$\boldsymbol{b} = \mu_0 \left(\boldsymbol{g}^{-1}\boldsymbol{h} + \boldsymbol{m}\right)\ . \tag{27}$$

Based on (27), and by consistency with the mapping relations derived for $\boldsymbol{b}$ and $\boldsymbol{h}$ above and visualized in Figure 14, it is concluded that the *material magnetization field* $\boldsymbol{M}$ is defined via the mapping $\boldsymbol{M} := J\boldsymbol{F}^{-1}\boldsymbol{m}$. Note that $\boldsymbol{m}$ transforms in the same manner as $\boldsymbol{b}$. The equivalent of relation (27) in the Lagrangian setting is thus given by

$$\boldsymbol{B} = \mu_0 \left(J\boldsymbol{C}^{-1}\boldsymbol{H} + \boldsymbol{M}\right)\ . \tag{28}$$

3.3.2. Extended Balance Laws of Continuum Thermodynamics. For any *admissible thermo-magneto-mechanical process* the following global balance laws must hold for every part $\mathcal{P}_t \subset \mathcal{S}$ of the material body, along with the Maxwell equations introduced in the previous section. These balance equations contain, in addition to the classical contributions, the *ponderomotive body force field* $\rho\boldsymbol{\gamma}^m(\boldsymbol{x},t)$, the *ponderomotive body couple field* $\rho\boldsymbol{l}^m(\boldsymbol{x},t)$ and the *magnetic energy source field* $\rho r^m(\boldsymbol{x},t)$, which are due to the *field-matter-interactions* of the deforming magnetizable body and the magnetic field.[4]

In the following equations $\mathfrak{M}$ denotes the *mass*, $\mathfrak{L}$ the *linear momentum*, $\mathfrak{F}$ the *resultant magnetomechanical force*, $\mathcal{A}_0$ the *angular momentum* and $\mathfrak{M}_0$ the *resultant magnetomechanical moment* about the origin, $\mathfrak{K}$ the *kinetic energy*, $\mathfrak{E}$ the *internal energy*, $\mathfrak{P}$ the *power due to external magnetomechanical forces*, $\mathfrak{Q}^h$ the *thermal power*, $\mathfrak{Q}^m$ the *additional*

[4]The specific form of electromagnetic source terms depends on the underlying model for field matter interactions, such as the *dipole–dipole*, or the *dipole–current loop* models discussed for example in [15], [27].

magnetic power[5], Γ the *total rate of entropy production*, $\mathfrak{H}$ the *entropy* and finally $\mathfrak{S}$ the *entropy power* of the considered part $\mathcal{P}_t$. We further introduce the *spatial mass density field* $\rho(\boldsymbol{x},t)$, the *spatial velocity field* $\boldsymbol{v}(\boldsymbol{x},t) := \partial_t \boldsymbol{\varphi}(\boldsymbol{X},t) \circ \boldsymbol{\varphi}_t^{-1}(\boldsymbol{x})$, the mass specific *mechanical body forces* $\rho\boldsymbol{\gamma}(\boldsymbol{x},t)$, the *internal energy density* per unit mass $e(\boldsymbol{x},t)$, the mass specific *heat source* $r^h(\boldsymbol{x},t)$, the *surface heat flux vector* $\boldsymbol{q}(\boldsymbol{x},t)$, the *entropy production* per unit mass $\gamma(\boldsymbol{x},t)$, the mass specific *entropy* $\eta(\boldsymbol{x},t)$ and the *absolute temperature field* $\theta(\boldsymbol{x},t)$.

With these definitions at hand, one can express the *global balance laws of continuum thermodynamics for magnetizable media in the spatial setting* in the following form

Balance of mass

$$\frac{d}{dt}\mathfrak{M} = 0 \ , \quad \frac{d}{dt}\int\limits_{\mathcal{P}_t} \rho \, dv = 0 \ . \tag{29a}$$

Balance of linear momentum

$$\frac{d}{dt}\mathfrak{L} = \mathfrak{F} \ , \quad \frac{d}{dt}\int\limits_{\mathcal{P}_t} \rho\boldsymbol{v} \, dv = \int\limits_{\mathcal{P}_t} \left[\rho\boldsymbol{\gamma} + \rho\boldsymbol{\gamma}^m\right] \, dv + \int\limits_{\partial\mathcal{P}_t} \boldsymbol{t} \, da \ . \tag{29b}$$

Balance of angular momentum

$$\frac{d}{dt}\mathfrak{A}_0 = \mathfrak{M}_0 \ , \quad \frac{d}{dt}\int\limits_{\mathcal{P}_t} \boldsymbol{x} \times \rho\boldsymbol{v} \, dv = \int\limits_{\mathcal{P}_t} \left[\boldsymbol{x} \times (\rho\boldsymbol{\gamma} + \rho\boldsymbol{\gamma}^m) + \rho\boldsymbol{l}^m\right] \, dv + \int\limits_{\partial\mathcal{P}_t} \boldsymbol{x} \times \boldsymbol{t} \, da \ . \tag{29c}$$

Balance of energy (first law of thermodynamics)

$$\frac{d}{dt}\left(\mathfrak{K} + \mathfrak{E}\right) = \mathfrak{P} + \mathfrak{Q}^h + \mathfrak{Q}^m \ , \tag{29d}$$

$$\frac{d}{dt}\int\limits_{\mathcal{P}_t} \left[\tfrac{1}{2}\,\rho\boldsymbol{v}\cdot\boldsymbol{g}\boldsymbol{v} + \rho e\right] \, dv = \int\limits_{\mathcal{P}_t} \left[(\rho\boldsymbol{\gamma} + \rho\boldsymbol{\gamma}^m)\cdot\boldsymbol{g}\boldsymbol{v}\right] \, dv + \int\limits_{\partial\mathcal{P}_t} \boldsymbol{t}\cdot\boldsymbol{g}\boldsymbol{v} \, da + \int\limits_{\mathcal{P}_t} \rho r^h \, dv - \int\limits_{\partial\mathcal{P}_t} \boldsymbol{q}\cdot\boldsymbol{n} \, da + \int\limits_{\mathcal{P}_t} \rho r^m \, dv \ .$$

Entropy inequality (second law of thermodynamics)

$$\Gamma := \frac{d}{dt}\mathfrak{H} - \mathfrak{S} \geq 0 \ , \quad \int\limits_{\mathcal{P}_t} \rho\gamma \, dv := \frac{d}{dt}\int\limits_{\mathcal{P}_t} \rho\eta \, dv - \left(\int\limits_{\mathcal{P}_t} \frac{\rho r^h}{\theta} \, dv - \int\limits_{\partial\mathcal{P}_t} \frac{\boldsymbol{q}\cdot\boldsymbol{n}}{\theta} \, da\right) \geq 0 \ . \tag{29e}$$

By using standard divergence, transport and localization theorems as well as the geometric mappings introduced above, the *local balance laws of continuum thermodynamics for magnetizable media in the spatial and material settings* are derived as

Balance of mass

$$\dot{\rho} + \rho \operatorname{div} \boldsymbol{v} = 0 \ , \qquad J\rho(\boldsymbol{\varphi}_t(\boldsymbol{X}),t) = \rho_0(\boldsymbol{X}) \ . \tag{30a}$$

[5]We follow here the approach of Pao & Hutter [27] and include the work done by the magnetic body couple $\rho\boldsymbol{l}^m$ in the source term ρr^m.

Balance of linear momentum

$$\rho\dot{\boldsymbol{v}} = \operatorname{div}\boldsymbol{\sigma} + \rho\boldsymbol{\gamma} + \rho\boldsymbol{\gamma}^m \ , \qquad \rho_0\dot{\boldsymbol{V}} = \operatorname{Div}\boldsymbol{P} + \rho_0\boldsymbol{\Gamma} + \rho_0\boldsymbol{\Gamma}^m \ . \tag{30b}$$

Balance of angular momentum

$$\operatorname{skew}\boldsymbol{\sigma} = \rho\boldsymbol{L}^m \ , \qquad \operatorname{skew}\left(\boldsymbol{P}\boldsymbol{F}^T\right) = \rho_0\boldsymbol{L}^m \ . \tag{30c}$$

Balance of energy (first law of thermodynamics)

$$\rho\dot{e} = \boldsymbol{\sigma} : \boldsymbol{g}\boldsymbol{l} + \rho r^h - \operatorname{div}\boldsymbol{q} + \rho r^m \ , \qquad \rho_0\dot{e} = \boldsymbol{g}\boldsymbol{P} : \dot{\boldsymbol{F}} + \rho_0 R^h - \operatorname{Div}\boldsymbol{Q} + \rho_0 R^m \ . \tag{30d}$$

Entropy inequality (second law of thermodynamics)

$$\rho\gamma = \rho\dot{\eta} - \rho\,\frac{r^h}{\theta} + \frac{1}{\theta}\operatorname{div}\boldsymbol{q} - \frac{1}{\theta^2}\,\boldsymbol{q}\cdot\operatorname{grad}\theta \geq 0 \ , \tag{30e}$$

$$\rho_0\gamma = \rho_0\dot{\eta} - \rho_0\,\frac{R^h}{\theta} + \frac{1}{\theta}\operatorname{Div}\boldsymbol{Q} - \frac{1}{\theta^2}\,\boldsymbol{Q}\cdot\operatorname{Grad}\theta \geq 0 \ . \tag{30f}$$

In the material setting we have defined the *reference mass density field* $\rho_0(\boldsymbol{X})$, the *material velocity field* $\boldsymbol{V}(\boldsymbol{X},t) := \partial_t\boldsymbol{\varphi}(\boldsymbol{X},t)$, the *material body force term* $\boldsymbol{\Gamma}^{(m)} := \boldsymbol{\gamma}^{(m)}(\boldsymbol{x},t)\circ\boldsymbol{\varphi}_t(\boldsymbol{X})$, the *material heat source* $R^{(m)} := r^{(m)}(\boldsymbol{x},t)\circ\boldsymbol{\varphi}_t(\boldsymbol{X})$ and, using the area map, the *material heat flux vector* $\boldsymbol{Q} := J\boldsymbol{q}\boldsymbol{F}^{-T}$. The tensor $\rho\boldsymbol{L}^m$ in the angular momentum balance is the *dual* of the body couple $\rho\boldsymbol{l}^m$ and defined through the relation $\boldsymbol{L}^m\boldsymbol{a} = -\frac{1}{2}\,\boldsymbol{l}^m\times\boldsymbol{a}$, $\forall\boldsymbol{a}$.

The balance laws for magnetizable continua listed above are general. As mentioned, however, they require the specification of the ponderomotive force and couple terms as well as the magnetic energy source term. These terms must be justified based on a particular field-matter-interactions theory. For a broader discussion of this deep subject the reader is referred to [15]. In this work, we briefly mention the following two approaches. The approach originally due to Lorentz [23], which was further developed by Dixon & Eringen [8, 9] and Eringen & Maugin [13], relies on the evaluation of the interactions of elementary electrically-charged particles in a volume element with electromagnetic fields, followed by a homogenization procedure, based on volume or phase-space averaging, to derive the desired continuum model. The model that will be adopted here, mainly because of its intuitiveness, mathematical simplicity and the resulting "symmetry" of electric and magnetic effects, is the *two-dipole model* in the so-called *Chu Formulation*, as discussed in detail by Penfield & Haus [28] and Hutter & van de Ven [27].

The two dipole model is built on the following three assumptions (cf. [15]):

(i) each material particle is equipped with a number of mutually noninteracting electric and magnetic dipoles,

(ii) each monopole experiences an electromagnetic body force as described by the *Lorentz force* $\rho\boldsymbol{F}^L := q^e\boldsymbol{e} + \mu_0 q^e\boldsymbol{v}\times\boldsymbol{h} + q^m\boldsymbol{h} - \varepsilon_0 q^m\boldsymbol{v}\times\boldsymbol{e}$, where q^e and q^m are the electric and (fictitious) magnetic charges of the monopoles later respectively related to the polarization and magnetization of an elementary volume, and

(iii) the monopoles of a particular dipole are only a small distance apart so that Taylor series expansions are justified.

Restricting ourselves to purely magnetic effects for the present purpose, the field-matter-interaction source terms of the (two)-dipole model are given by [15]

$$\rho\boldsymbol{\gamma}^m = \mu_0\,(\operatorname{grad}\boldsymbol{h})\,\boldsymbol{m} \ , \quad \rho\boldsymbol{L}^m = \mu_0\operatorname{skew}\left[\boldsymbol{m}\otimes\boldsymbol{h}\right] \ , \quad \rho r^m = \rho\boldsymbol{h}\cdot\frac{d}{dt}\left(\frac{\mu_0\boldsymbol{m}}{\rho}\right) \ . \tag{31}$$

3.3.3. The Maxwell Stress Tensor Concept. It is often convenient to reformulate the balance of momentum equations in terms of spatial Cauchy-type *Maxwell stress tensor* $\boldsymbol{\sigma}^M$. This second order tensor is defined such that $\operatorname{div}\boldsymbol{\sigma}^M = \rho\boldsymbol{\gamma}^m$ and $\operatorname{skew}\boldsymbol{\sigma}^M = -\rho\boldsymbol{L}^m$. Further defining the *total stress tensor* $\boldsymbol{\sigma}^t := \boldsymbol{\sigma} + \boldsymbol{\sigma}^M$, it then directly follows that $(30\text{b})_1$ and $(30\text{c})_1$ can be rewritten in the following form[6]

$$\operatorname{div}\boldsymbol{\sigma}^t + \rho\boldsymbol{\gamma} = \boldsymbol{0} \ , \qquad \operatorname{skew}\boldsymbol{\sigma}^t = \boldsymbol{0} \ , \tag{32}$$

such that the total Cauchy-stress tensor is again *symmetric* and the balance of angular momentum is trivially satisfied. For the (two)-dipole model the Maxwell stress tensor takes the form $\boldsymbol{\sigma}^M := \boldsymbol{g}^{-1}\boldsymbol{h}\otimes\boldsymbol{b} - \frac{1}{2}\,\mu_0\,(\boldsymbol{h}\cdot\boldsymbol{g}^{-1}\boldsymbol{h})\,\boldsymbol{1}$. It is easily verified that this definition is consistent with the ponderomotive force and couple expressions given in $(31)_{1,2}$.

Similarly, with $\boldsymbol{P}^t := \boldsymbol{P} + \boldsymbol{P}^M$ and $\boldsymbol{P}^M := \boldsymbol{\varphi}^*(J\boldsymbol{\sigma}^M) = J\boldsymbol{\sigma}^M\boldsymbol{F}^{-T}$ one obtains in the Lagrangian setting

$$\operatorname{Div}\boldsymbol{P}^t + \rho_0\boldsymbol{\Gamma} = \boldsymbol{0} \ , \qquad \operatorname{skew}\left[\boldsymbol{P}^t\boldsymbol{F}^T\right] = \boldsymbol{0} \ . \tag{33}$$

For the (two)-dipole model the *material Maxwell-type first Piola-Kirchhoff stress tensor* can be written in the form

$$\boldsymbol{g}\boldsymbol{P}^M = \boldsymbol{F}^{-T}\boldsymbol{H}\otimes\boldsymbol{B} - \tfrac{1}{2}\,J\mu_0\left[\boldsymbol{C}^{-1} : (\boldsymbol{H}\otimes\boldsymbol{H})\right]\boldsymbol{F}^{-T} \tag{34}$$

.

3.4. Thermodynamically-Consistent Constitutive Theory

A continuum constitutive theory is considered to be *thermodynamically-consistent* if it satisfies the fundamental balance equations of continuum mechanics and the laws of thermodynamics derived in the previous section at each material point (see also Coleman & Noll [5]). It is assumed that all thermodynamic properties of the material can be characterized by a (scalar-valued) *thermodynamic potential*, such as the *specific internal energy* previously introduced in the energy balance (29d). Following the *Coleman and Noll method* it is possible to derive general constitutive relations for the dependent field variables in the form of gradients to the thermodynamic potential, such that thermodynamic consistency is guaranteed a priori. To this end, one requests that the thermodynamic potential satisfy the *Clausius-Duhem inequality* for all admissible thermodynamic processes. In the case of inelastic response, a reduced form of the inequality additionally constrains the evolution of internal state variables.

The specific form of the Clausius-Duhem inequality depends on the choice of thermodynamic potential. The internal energy form in the material setting follows by substituting the energy balance $(30\text{d})_2$ into the entropy inequality (30f) as

$$J\mathcal{D} := \rho_0\gamma\theta = \rho_0\dot{\eta}\theta + \boldsymbol{g}\boldsymbol{P} : \dot{\boldsymbol{F}} - \rho_0\dot{e} + \rho_0 R^m - \frac{1}{\theta}\boldsymbol{Q}\cdot\operatorname{Grad}\theta \geq 0 \ , \tag{35}$$

[6] In mechanics it is typically straightforward to distinguish *near-field effects*, i.e. the mechanical interaction of a part with the cut-off remainder of the body, and *far-field effects*, such as the volumetric force exerted on the body by the gravitational field. In the mechanics of electromagnetic continua, however, this distinction is much more subtle and leads to the *non-uniqueness* of stress tensor definitions. In the approach presented here, for example, one completely accounts for the far-field-type electromagnetic interactions through Maxwell's stress tensor, whose divergence is actually a measure of the near-field interactions (see also discussion in [15]). Furthermore, one may add any divergence-free tensor field to the chosen form of Maxwell's stress tensor, without changing the corresponding equations of motion (32), except of course in terms of the jump conditions on the boundary (cf. ??).

where $J\mathcal{D}$ denotes the *dissipation* per unit reference volume. The dissipation may be split into a local contribution $J\mathcal{D}_{loc} := \rho_0\dot{\eta}\theta + \boldsymbol{g}\boldsymbol{P} : \dot{\boldsymbol{F}} - \rho_0\dot{e} + \rho_0 R^m$ and a contribution due to heat conduction $J\mathcal{D}_{con} := -\frac{1}{\theta}\boldsymbol{Q}\cdot\operatorname{Grad}\theta$, and one typically enforces the stronger restriction that each of these terms individually be non-negative, which gives rise to the *Clausius-Planck-inequality* $\mathcal{D}_{loc} \geq 0$ and the *Fourier inequality* $\mathcal{D}_{con} \geq 0$.

An alternative form of the Clausius-Planck-inequality can be derived by introducing the *free energy-enthalpy function* $\hat{\psi}^*$ via the *partial Legendre transformation*[7]

$$\rho_0\hat{\psi}^*(\boldsymbol{F},\boldsymbol{H},\theta) := \rho_0\hat{e}(\boldsymbol{F},\mu_0\boldsymbol{M},\eta) - \boldsymbol{H}\cdot\mu_0\boldsymbol{M} - \rho_0\theta\eta \ . \tag{36}$$

Computing the rate of change of the specific internal energy from (36) and substituting the resulting expression into (35) along with the magnetic energy source term $(31)_3$, which in the Lagrangian setting takes the form $\rho_0 R^m = \boldsymbol{H}\cdot\mu_0\dot{\boldsymbol{M}} + \big(\boldsymbol{F}^{-T}\boldsymbol{H}\otimes\mu_0\boldsymbol{M}\big) : \dot{\boldsymbol{F}}$, yields the free energy-enthalpy form of the Clausius-Planck inequality for finite magnetomechanics

$$J\mathcal{D}_{loc} = \big[\boldsymbol{g}\boldsymbol{P} + \boldsymbol{F}^{-T}(\boldsymbol{H}\otimes\mu_0\boldsymbol{M})\big] : \dot{\boldsymbol{F}} - \mu_0\boldsymbol{M}\cdot\dot{\boldsymbol{H}} - \rho_0\eta\dot{\theta} - \rho_0\dot{\hat{\psi}}^* \geq 0 \ . \tag{37}$$

For thermodynamically-reversible processes, when no internal state variables are included, the rate of $\hat{\psi}^*$ is given by $\dot{\hat{\psi}}^* = \partial_{\boldsymbol{F}}\hat{\psi}^* : \dot{\boldsymbol{F}} + \partial_{\boldsymbol{H}}\hat{\psi}^*\cdot\dot{\boldsymbol{H}} + \partial_\theta\hat{\psi}^*\cdot\dot{\theta}$ and the inequality (37) reduces to the equality

$$\Big[\boldsymbol{g}\boldsymbol{P} + \boldsymbol{F}^{-T}(\boldsymbol{H}\otimes\mu_0\boldsymbol{M}) - \rho_0\partial_{\boldsymbol{F}}\hat{\psi}^*\Big] : \dot{\boldsymbol{F}} - \Big[\mu_0\boldsymbol{M} + \rho_0\partial_{\boldsymbol{H}}\hat{\psi}^*\Big]\cdot\dot{\boldsymbol{H}} - \rho_0\Big[\eta + \partial_\theta\hat{\psi}^*\Big]\dot{\theta} \stackrel{!}{=} 0. \tag{38}$$

Following the Coleman and Noll argumentation, that the individual terms in (38) are linear in the rates of the state variables, but their coefficients are by the constitutive assumptions independent of those rates, and requesting that the equality hold for all admissible processes involving independent changes of the state variables, the following general constitutive equations are deduced

$$\boxed{\boldsymbol{g}\boldsymbol{P} = \rho_0\partial_{\boldsymbol{F}}\hat{\psi}^* - \boldsymbol{F}^{-T}(\boldsymbol{H}\otimes\mu_0\boldsymbol{M}) \ , \quad \mu_0\boldsymbol{M} = -\rho_0\partial_{\boldsymbol{H}}\hat{\psi}^* \ , \quad \eta = \partial_\theta\hat{\psi}^* \ .} \tag{39}$$

It should be pointed out that the free energy-enthalpy function introduced above can be attributed to the energy storage in the magnetizable and deformable thermoelastic solid. Since, however, in electromagnetism energy is also stored in the free space occupied by the material body, it is often convenient to reinterpret the energy balance by introducing the *amended free energy-enthalpy function* (cf. Dorfmann & Ogden [11])

$$\Psi^* = \hat{\Psi}^*(\boldsymbol{F},\boldsymbol{H}) = \hat{\psi}^*(\boldsymbol{F},\boldsymbol{H}) + \hat{\psi}^{*,free}(\boldsymbol{H}) \ , \tag{40}$$

which explicitly contains contributions related to the energy storage in matter and free space. The free space energy storage is assumed as

$$\rho_0\hat{\psi}^{*,free}(\boldsymbol{H}) = -\frac{1}{2}\mu_0 J\boldsymbol{h}\cdot\boldsymbol{g}^{-1}\boldsymbol{h} = -\frac{1}{2}\mu_0 J\boldsymbol{C}^{-1} : (\boldsymbol{H}\otimes\boldsymbol{H}) \ . \tag{41}$$

[7] In the classical nomenclature of continuum thermomechanics $\psi = \hat{\psi}(\boldsymbol{F},\theta)$ denotes the *Helmholtz free energy*. In thermo-magneto-mechanics the free energy contains the magnetization or the magnetic induction, see discussion on the free space energy storage contribution below, as an additional independent state variable, i.e. $\psi = \hat{\psi}(\boldsymbol{F},\mu_0\boldsymbol{M},\theta)$. The thermodynamic potential $\psi^* = \hat{\psi}^*(\boldsymbol{F},\boldsymbol{H},\theta)$ is thus of free-energy-type in terms of the mechanical variable, but of free-enthalpy-type regarding the magnetic variable, and hence the term *free energy-enthalpy function* is used here (see [7] for the related discussion of the nomenclature in thermo-electro-mechanics, where the electric equivalent of this potential is referred to as the *electric Gibbs function*.)

Furthermore, its rate of change can be shown to result as

$$\rho_0\dot{\psi}^{*,free}(\boldsymbol{H}) = \left[-\frac{1}{2}\mu_0 J\left(\boldsymbol{C}^{-1}:(\boldsymbol{H}\otimes\boldsymbol{H})\right)\boldsymbol{F}^{-T} + \mu_0 J\left(\boldsymbol{F}^{-T}\boldsymbol{H}\otimes\boldsymbol{C}^{-1}\boldsymbol{H}\right)\right]:\dot{\boldsymbol{F}} - \mu_0 J\boldsymbol{C}^{-1}\boldsymbol{H}\cdot\dot{\boldsymbol{H}}\ . \tag{42}$$

Substitution of $-\rho_0\dot{\psi}^* = \rho_0\dot{\psi}^{*,free} - \rho_0\dot{\Psi}^*$, using (42), into the Clausius-Planck inequality (37) yields after some algebraic manipulations

$$J\mathcal{D}_{loc} = \left[\boldsymbol{g}\boldsymbol{P} + \boldsymbol{F}^{-T}\boldsymbol{H}\otimes\left(\mu_0\boldsymbol{M} + \mu_0 J\boldsymbol{C}^{-1}\boldsymbol{H}\right) - \frac{1}{2}\mu_0 J\left(\boldsymbol{C}^{-1}:(\boldsymbol{H}\otimes\boldsymbol{H})\right)\boldsymbol{F}^{-T}\right]:\dot{\boldsymbol{F}} - \mu_0\left[\boldsymbol{M} + J\boldsymbol{C}^{-1}\boldsymbol{H}\right]\cdot\dot{\boldsymbol{H}} - \rho_0\dot{\Psi}^*\ , \tag{43}$$

where isothermal conditions have been assumed for conciseness. Employing the constitutive relation (28) and recognizing the first Piola-Kirchhoff-type Maxwell stress tensor $\boldsymbol{g}\boldsymbol{P}^M$ from its definition (34), (43) takes the much simpler form

$$J\mathcal{D}_{loc} = \left[\boldsymbol{g}\boldsymbol{P} + \boldsymbol{g}\boldsymbol{P}^M\right]:\dot{\boldsymbol{F}} - \boldsymbol{B}\cdot\dot{\boldsymbol{H}} - \rho_0\dot{\Psi}^* = 0\ . \tag{44}$$

Substituting the rate $\dot{\Psi}^* = \partial_{\boldsymbol{F}}\hat{\Psi}^* : \dot{\boldsymbol{F}} + \partial_{\boldsymbol{H}}\hat{\Psi}^*\cdot\dot{\boldsymbol{H}}$ and again following the Coleman and Noll argument, we arrive at the alternative set of general constitutive equations

$$\boxed{\boldsymbol{g}\boldsymbol{P}^t = \rho_0\partial_{\boldsymbol{F}}\hat{\Psi}^*\ , \quad \boldsymbol{B} = -\rho_0\partial_{\boldsymbol{H}}\hat{\Psi}^*\ .} \tag{45}$$

The constitutive equation for the total first Piola-Kirchhoff stress tensor is thus given simply in terms of the partial gradient of the amended energy-enthalpy function with respect to the deformation gradient. Likewise, the partial gradient with respect to the Lagrangian magnetic field yields the constitutive equation for the magnetic induction in the material setting, with contributions from the field matter interactions as well as free space. Relations (45) represent the basis for the construction of specific constitutive models of finite magnetoelasticity presented in Section 5. It should also be pointed out that many other variations of thermodynamically-consistent constitutive equations, resulting mainly from different choices of the set of independent state variables, have been discussed in the literature (see e.g. Kankanala & Triantafyllidis [19] or Dorfmann & Ogden [12] for overviews.)

In addition to the requirement of thermodynamic consistency discussed above, the constitutive equations must also satisfy the requirements of *material objectivity* and *material symmetry*. The *principle of material objectivity (PMO)*, also referred to as *principle of material frame-invariance*, requires that the material response be invariant under changes in observer (see e.g. Gurtin [14]). From the so-called *active viewpoint*, this requirement is equivalent to the statement that the energy stored in the system ought to be unaffected by rigid-body motions of the form $\boldsymbol{r}_t = \boldsymbol{Q}(t)\boldsymbol{x} + \boldsymbol{c}(t)$ superimposed onto the current configuration. Here, the proper orthogonal tensor $\boldsymbol{Q}(t)\in\mathcal{SO}(3)$ represents a time-dependent rotation and the vector $\boldsymbol{c}(t)$ a time-dependent translation. Consequently, the deformation gradient $\boldsymbol{F}^*$, which maps tangents to material curves onto tangents of the deformed and rigidly translated and rotated material curves, takes the form $\boldsymbol{F}^* = \boldsymbol{Q}\boldsymbol{F}$.

The material magnetic field $\boldsymbol{H}$, however, is unaffected by observer transformations in the current configuration, since it is a Lagrangian field variable. For finite magnetoelasticity in the two-point setting, the amended free energy-enthalpy function $\Psi^* = \hat{\Psi}^*(\boldsymbol{F}, \boldsymbol{H})$ must therefore additionally comply with the constraint

$$\hat{\Psi}^*(\boldsymbol{F}^*, \boldsymbol{H}^*) = \hat{\Psi}^*(\boldsymbol{Q}\boldsymbol{F}, \boldsymbol{H}) \stackrel{!}{=} \hat{\Psi}^*(\boldsymbol{F}, \boldsymbol{H}) \ , \quad \forall\, \boldsymbol{Q} \in \mathcal{SO}(3) \ . \tag{46}$$

In order to satisfy the objectivity requirement *a priori*, one can introduce the *reduced form* of the free energy-enthalpy function[8]

$$\Psi^* = \hat{\Psi}^*(\boldsymbol{C}(\boldsymbol{F}), \boldsymbol{H}) = \hat{\Psi}^*\left(\boldsymbol{F}^T\boldsymbol{g}\boldsymbol{F}, \boldsymbol{H}\right) \ . \tag{47}$$

With the orthogonality relation $\boldsymbol{Q}^T\boldsymbol{g}\boldsymbol{Q} = \boldsymbol{g}$, it then directly follows

$$\begin{aligned} \hat{\Psi}^*(\boldsymbol{C}^*(\boldsymbol{F}^*), \boldsymbol{H}^*) &= \hat{\Psi}^*\left((\boldsymbol{F}^*)^T\boldsymbol{g}\boldsymbol{F}^*, \boldsymbol{H}\right) = \hat{\Psi}^*\left(\boldsymbol{F}^T\boldsymbol{Q}^T\boldsymbol{g}\boldsymbol{Q}\boldsymbol{F}, \boldsymbol{H}\right) \\ &= \hat{\Psi}^*(\boldsymbol{F}^T\boldsymbol{g}\boldsymbol{F}, \boldsymbol{H}) = \hat{\Psi}^*(\boldsymbol{C}(\boldsymbol{F}), \boldsymbol{H}) \ . \end{aligned} \tag{48}$$

Textured and untextured poly-crystals, single-crystalline materials, many composites and also materials with imposed directions of polarization or magnetization exhibit symmetries in their *microstructure* that must be taken into account in the construction of constitutive models predicting their response. Furthermore, for magnetorheological elastomers, which, as discussed, are essentially composites consisting of micron-sized magnetizable particles embedded in an elastomeric matrix material, we expect the response and thus the energy-enthalpy function to be independent of the sign of the magnetic field, i e.

$$\hat{\Psi}^*(\boldsymbol{C}, \boldsymbol{H}) \stackrel{!}{=} \hat{\Psi}^*(\boldsymbol{C}, -\boldsymbol{H}) \ , \tag{49}$$

which is automatically satisfied if one assumes

$$\hat{\Psi}^*(\boldsymbol{C}, \boldsymbol{H}) = \hat{\Psi}^*(\boldsymbol{C}, \boldsymbol{H} \otimes \boldsymbol{H}) \ . \tag{50}$$

The *principle of material symmetry* states that locally the free energy-enthalpy function ought to be invariant with respect to rotations $\boldsymbol{Q}$ superimposed onto the open neighborhood $\mathcal{N}_X \subset \mathcal{B}$ of a material point $\boldsymbol{X}$ in the reference configuration, in case these rotations are elements of the appropriate *material symmetry group* $\mathcal{G} \subset \mathcal{SO}(3)$. Or in other words, a magnetomechanical experiment involving the considered material should make no distinction between symmetry-related reference states. For the objective reduced form of the free energy-enthalpy function this requirement is mathematically expressed as (see also the discussion by Steigmann [30])

$$\hat{\Psi}^*(\boldsymbol{C}^*, \boldsymbol{H}^*) = \hat{\Psi}^*(\boldsymbol{Q}\boldsymbol{C}\boldsymbol{Q}^T, \boldsymbol{Q}\boldsymbol{H}) \stackrel{!}{=} \hat{\Psi}^*(\boldsymbol{C}, \boldsymbol{H}) \ , \quad \forall\, \boldsymbol{Q} \in \mathcal{G} \subset \mathcal{SO}(3) \ . \tag{51}$$

Note that for an isotropic material the symmetry group is identical to the set of all rotations, i.e. $\mathcal{G} \equiv \mathcal{SO}(3)$. From the combination of (50) and (51), one thus demands that the free energy-enthalpy function, in order to satisfy objectivity, material symmetry and invariance with respect to the sign of the magnetic field, satisfy the following constraint

$$\hat{\Psi}^*\left(\boldsymbol{Q}\boldsymbol{C}\boldsymbol{Q}^T, \boldsymbol{Q}(\boldsymbol{H} \otimes \boldsymbol{H})\boldsymbol{Q}^T\right) \stackrel{!}{=} \hat{\Psi}^*(\boldsymbol{C}, \boldsymbol{H} \otimes \boldsymbol{H}) \ , \quad \forall\, \boldsymbol{Q} \in \mathcal{G} \ . \tag{52}$$

[8]Note that to keep the notation manageable, we have refrained from introducing another symbol for the reduced form of the free energy-enthalpy function. The same policy will henceforth be followed where appropriate.

3.5. Fully-Coupled Boundary Value Problems

There exist two common approaches to solving boundary value problems in magnetostatics. The *scalar potential formulation* is based on the idea that, in the absence of free electric currents, one can identically satisfy Ampère's law, for example in the form of $(26b)_2$, by deriving the magnetic field from a scalar-valued potential Φ according to $\boldsymbol{H} = -\operatorname{Grad}\Phi$. One observes that $\operatorname{Curl}\boldsymbol{H} = -\operatorname{Curl}(\operatorname{Grad}\Phi) = \boldsymbol{0}$, since potential fields (gradient fields) are curl-free (irrotational).[9] Problems involving general free volumetric and surface electric current fields may be solved on the basis of a *vector potential formulation*, in which the magnetic induction is defined as the curl of a vector-valued magnetic potential $\boldsymbol{\Phi}$, i.e. $\boldsymbol{B} = \operatorname{Curl}\boldsymbol{\Phi}$. This definition identically satisfies the Gauss-Faraday law in the form of $(26a)_2$, i.e. $\operatorname{Div}(\operatorname{Curl}\boldsymbol{\Phi}) = 0$, since curl fields are divergence-free (i.e. source/sink-free or solenoidal). While being more general, vector potential formulations suffer from the disadvantage of non-uniqueness in three dimensional problems and their solutions may contain spurious components (see e.g. [16, 29]). To overcome this problem, one must additionally specify appropriate *gauge conditions*, such as the commonly-used *Coulomb gauge* $\operatorname{Div}\boldsymbol{\Phi} = 0$, and enforce them for example via penalty-type methods. Furthermore, the boundary conditions for vector-potential-based magnetostatic problems are much more difficult to interpret from a physical standpoint. For these reasons, only scalar-potential formulations will be employed in this work.[10]

To complete the formulation of well-posed boundary value problems in finite magnetomechanics, appropriate boundary conditions must be specified. To this end, one considers the material body $\mathcal{B}$ depicted in Figure 15, whose surface is considered to be subdivided into the non-overlapping segments $\partial\mathcal{B}_{\boldsymbol{\varphi}}$ and $\partial\mathcal{B}_t$, such that $\partial\mathcal{B} = \partial\mathcal{B}_{\boldsymbol{\varphi}} \cup \partial\mathcal{B}_t$ and $\partial\mathcal{B}_{\boldsymbol{\varphi}} \cap \partial\mathcal{B}_t \in \emptyset$ from the mechanical viewpoint, and into the segments $\partial\mathcal{B}_\Phi$ and $\partial\mathcal{B}_B$, with $\partial\mathcal{B} = \partial\mathcal{B}_\Phi \cup \partial\mathcal{B}_B$ and $\partial\mathcal{B}_\Phi \cap \partial\mathcal{B}_B \in \emptyset$, in the magnetic case. There exists of course no general restrictions on how the mechanical and magnetic surface segments might overlap.

The appropriate *Dirichlet and Neumann-type* mechanical and magnetic *boundary conditions* to be applied to the respective boundary segments are given by

$$\begin{aligned} &\boldsymbol{\varphi} = \bar{\boldsymbol{\varphi}} \ , \quad \text{on } \partial\mathcal{B}_{\boldsymbol{\varphi}} \ , \qquad \boldsymbol{P}^t\boldsymbol{N} = \bar{\boldsymbol{t}}^{\,t} \ , \quad \text{on } \partial\mathcal{B}_t \ , \\ &\Phi = \bar{\Phi} \ , \quad \text{on } \mathcal{B}_\Phi \ , \qquad \boldsymbol{B}\cdot\boldsymbol{N} = \bar{B} \ , \quad \text{on } \partial\mathcal{B}_B \ . \end{aligned} \tag{53}$$

It has further been assumed, as depicted in Figure 15, that the body may contain a discontinuity surface Γ_d over which the magneto-mechanical field variables can suffer jumps. For the following considerations we restrict ourselves to *material surfaces*, i.e. surfaces that consist of material points and thus possess no relative velocity compared to the material coordinates. The appropriate *jump conditions* can directly be derived from

[9] In some cases the free current field may be simple enough, for example a spatially homogeneous current with a particular direction, that it is possible to also use the scalar-potential formulation by amending the potential in the form of $\Phi \to \Phi + \Phi^{J_f}$, where Φ^{J_f} is constructed such that its gradient is identical to the desired free current field.

[10] For homogeneous isotropic materials, described for example by the constitutive relation $\boldsymbol{B} = \mu\boldsymbol{H}$, where μ is the permeability of the material, the magnetostatic problem in the scalar-valued formulation reduces to the *Laplace equation* $\Delta\Phi = 0$ and consequently Φ is said to be *harmonic*. In the vector potential case one obtains, using the identity $\operatorname{Curl}(\operatorname{Curl}\boldsymbol{\Phi}) = \operatorname{Grad}(\operatorname{Div}\boldsymbol{\Phi}) - \boldsymbol{\Delta}\boldsymbol{\Phi}$, the inhomogeneous Laplace or *Poisson equation* $\mu^{-1}\Delta\boldsymbol{\Phi} = -\boldsymbol{J}_f$, where $\boldsymbol{\Delta}[\,\cdot\,]$ is the vector-valued Laplace operator. For current-free cases, $\boldsymbol{\Phi}$ satisfies the vectorial Laplace equation and is thus harmonic, which also implies that it is simultaneously divergence free (solenoidal) and curl-free (irrotational).

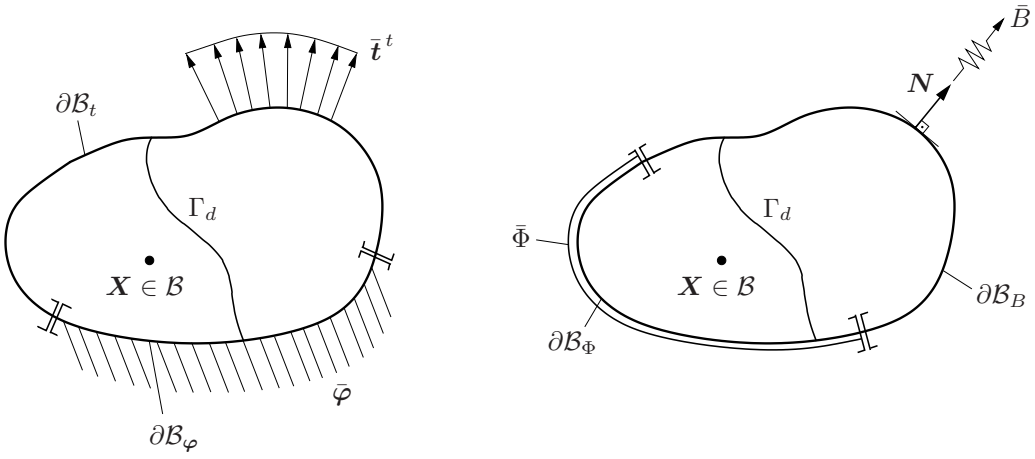

Figure 15: Visualization of the mechanical and magnetic boundary conditions on the surface segments $\partial\mathcal{B}=\partial\mathcal{B}_{\boldsymbol{\varphi}}\cup\partial\mathcal{B}_t$ or $\partial\mathcal{B}=\partial\mathcal{B}_\Phi\cup\partial\mathcal{B}_B$ of the body in the reference configuration.

the global balance laws introduced in the preceding sections, by considering a generic material volume containing a discontinuity surface and taking the limit as the volume goes to zero. In the material setting they are given by

$$[\![\boldsymbol{\varphi}]\!] = \boldsymbol{0} \ , \quad [\![\boldsymbol{P}^t]\!]\,\boldsymbol{N} = \boldsymbol{0} \ , \quad [\![\Phi]\!] = 0 \ , \quad [\![\boldsymbol{B}]\!]\cdot\boldsymbol{N} = 0 \ , \quad \text{on } \Gamma_d \ . \tag{54}$$

The notation is such that the jump of a scalar, vector or general tensor quantity $\boldsymbol{A}$ is defined as $[\![\boldsymbol{A}]\!] := \boldsymbol{A}^+ - \boldsymbol{A}^-$, where the sign superscript indicates the positive and negative side of the discontinuity surface with respect to the unit normal $\boldsymbol{N}$. It should be pointed out that the continuity condition $(54)_3$, imposed on the magnetic potential, also guarantees that the tangential component of the magnetic field is continuous over the interface. Note also that for material surfaces the boundary conditions (53) can be considered as special case of the jump conditions (54).

We have thus completed the derivation of the geometrically and physically-nonlinear problem of (static) magnetomechanics at finite strains. The complete set of the associated governing equations is summarized in Box 1.[11]

3.6. Variational Formulations of Finite Magnetoelasticity

Alternative approaches to the modeling of coupled boundary value problems in finite magnetomechanics can be derived by means of *variational principles*. Such approaches are not only advantageous due to their mathematical elegance and conciseness, but also because they naturally provide a basis for numerical methods, e.g. finite element discretizations, and automatically lead to symmetric tangent matrices, such that fast symmetric solvers can be employed in the numerical solution of the considered highly-nonlinear problems. With these advantages in mind, we consider the following *stationarity principle*

$$I(\boldsymbol{\varphi}, -\Phi) := \int_{\mathcal{B}} \hat{\Psi}^*\big(\boldsymbol{F}(\boldsymbol{\varphi}), \boldsymbol{H}(-\Phi)\big)\, dV - \int_{\partial\mathcal{B}_t} \bar{\boldsymbol{t}}^{\,t}\cdot\boldsymbol{\varphi}\, dA - \int_{\partial\mathcal{B}_B} \bar{B}\cdot\Phi\, dA \quad \longrightarrow \text{ stat.} \tag{56}$$

[11] The specific free energy-enthalpy function has now be redefined to be measured per unit reference volume, instead of per unit mass as before. For conciseness, we have refrained from introducing another symbol.

Box 1: Summary of the Finite Deformation Magnetomechanical Boundary Value Problem in the Two-Point Setting and Scalar Magnetic Potential Formulation.

1. Kinematics

$$\boldsymbol{F} = \operatorname{Grad} \boldsymbol{\varphi} \ , \qquad \boldsymbol{H} = -\operatorname{Grad} \Phi \ . \tag{55a}$$

2. Equilibrium equations/Gauss-Faraday law

$$\operatorname{Div} \boldsymbol{P}^t + \rho_0 \boldsymbol{\Gamma} = \boldsymbol{0} \ , \qquad \operatorname{Div} \boldsymbol{B} = 0 \ , \quad \text{in } \mathcal{B} \ . \tag{55b}$$

3. Constitutive relations

$$\boldsymbol{g}\boldsymbol{P}^t = \partial_{\boldsymbol{F}} \hat{\Psi}^*(\boldsymbol{C}(\boldsymbol{F}), \boldsymbol{H}) \qquad \boldsymbol{B} = -\partial_{\boldsymbol{H}} \hat{\Psi}^*(\boldsymbol{C}(\boldsymbol{F}), \boldsymbol{H}) \ . \tag{55c}$$

4. Boundary conditions

$$\begin{aligned} &\boldsymbol{\varphi} = \bar{\boldsymbol{\varphi}} \ , \quad \text{on } \partial\mathcal{B}_{\boldsymbol{\varphi}} \ , \qquad \boldsymbol{P}^t \boldsymbol{N} = \bar{\boldsymbol{t}}^{\,t} \ , \quad \text{on } \partial\mathcal{B}_t \ , \\ &\Phi = \bar{\Phi} \ , \quad \text{on } \mathcal{B}_\Phi \ , \qquad \boldsymbol{B} \cdot \boldsymbol{N} = \bar{B} \ , \quad \text{on } \partial\mathcal{B}_B \ . \end{aligned} \tag{55d}$$

5. Interface jump conditions

$$\begin{aligned} &[\![\boldsymbol{\varphi}]\!] = \boldsymbol{0} \ , \quad [\![\boldsymbol{P}^t]\!]\, \boldsymbol{N} = \boldsymbol{0} \ , \quad [\![\Phi]\!] = 0 \ , \\ &[\![\boldsymbol{B}]\!] \cdot \boldsymbol{N} = 0 \ , \quad \text{on } \Gamma_d \ . \end{aligned} \tag{55e}$$

It is demonstrated in Appendix A that the *Euler-Lagrange equations* of the variational problem (56) coincide with the field equations and boundary conditions of the magnetomechanical problem (55) summarized in Box 1 in Section 3.5.

The necessary condition for the stationarity of (56) requires that its first variation vanish. Using the definitions $\delta\boldsymbol{F} = \operatorname{Grad} \delta\boldsymbol{\varphi}$ and $\delta\boldsymbol{H} = \operatorname{Grad} \delta(-\Phi)$, and enforcing the *essential boundary conditions* $\boldsymbol{\varphi} = \bar{\boldsymbol{\varphi}}$ on $\partial\mathcal{B}_{\boldsymbol{\varphi}}$ and $\Phi = \bar{\Phi}$ on $\partial\mathcal{B}_\Phi$, one obtains the following expression

$$\begin{aligned} \delta I(\boldsymbol{\varphi}, \delta\boldsymbol{\varphi}, -\Phi, \delta(-\Phi)) = &\int_{\mathcal{B}} \left[\partial_{\boldsymbol{F}} \hat{\Psi}^* : \operatorname{Grad} \delta\boldsymbol{\varphi} + \partial_{\boldsymbol{H}} \hat{\Psi}^* \cdot \operatorname{Grad} \delta(-\Phi) \right] dV \\ &- \int_{\partial\mathcal{B}_t} \bar{\boldsymbol{t}}^{\,t} \cdot \delta\boldsymbol{\varphi} \, dA + \int_{\partial\mathcal{B}_B} \bar{B} \cdot \delta(-\Phi) \ dA \stackrel{!}{=} 0 \ . \end{aligned} \tag{57}$$

Note that (57) represents the *weak form* of the coupled problem on the basis of which the finite element model will be constructed in Section 4. One may also interpret (57) as the specific form of the *principle of virtual work* for the considered problem. The first term

on the right-hand-side of (57) then represents the internal virtual work associated with changes in the material and free space energy storage due to virtual changes of $\boldsymbol{F}$ and (negative) Φ. The remaining terms represent the associated external virtual work of the prescribed traction and normal component of the magnetic induction fields, respectively.

To find the roots of the geometrically- and physically-nonlinear problem (57) one typically employs a *Newton-Raphson-type iteration scheme*, for which one must compute the *linearization* of the weak form. Defining $G := \delta I$ to simplify the notation, assuming that the prescribed surface tractions and magnetic induction components are independent of the deformation (i.e. dead loads), and linearizing the weak form about the point $\big(\bar{\boldsymbol{\varphi}}, \delta\bar{\boldsymbol{\varphi}}, -\bar{\Phi}, \delta\big(-\bar{\Phi}\big)\big)$, it follows

$$\begin{aligned}\operatorname{Lin} G\left(\bar{\boldsymbol{\varphi}}, \delta\bar{\boldsymbol{\varphi}}, \Delta\boldsymbol{\varphi}, -\bar{\Phi}, \delta\big(-\bar{\Phi}\big), \Delta\big(-\bar{\Phi}\big)\right) &= G\left(\bar{\boldsymbol{\varphi}}, \delta\bar{\boldsymbol{\varphi}}, -\bar{\Phi}, \delta\big(-\bar{\Phi}\big)\right) \\ &\quad + \Delta_{\boldsymbol{\varphi}} G\left(\bar{\boldsymbol{\varphi}}, \delta\bar{\boldsymbol{\varphi}}, \Delta\boldsymbol{\varphi}, -\bar{\Phi}, \delta\big(-\bar{\Phi}\big)\right) \\ &\quad + \Delta_{(-\Phi)} G\left(\bar{\boldsymbol{\varphi}}, \delta\bar{\boldsymbol{\varphi}}, -\bar{\Phi}, \delta\big(-\bar{\Phi}\big), \Delta\big(-\bar{\Phi}\big)\right) ,\end{aligned} \tag{58}$$

where the increments are specifically given by

$$\Delta_{\boldsymbol{\varphi}} G = \int_{\mathcal{B}} \Big[\operatorname{Grad}\delta\boldsymbol{\varphi} : \partial^2_{\boldsymbol{FF}}\hat{\Psi}^* : \operatorname{Grad}\Delta\boldsymbol{\varphi} + \operatorname{Grad}\delta(-\Phi) : \partial^2_{\boldsymbol{HF}}\hat{\Psi}^* : \operatorname{Grad}\Delta\boldsymbol{\varphi}\Big] dV, \tag{59}$$

$$\Delta_{(-\Phi)} G = \int_{\mathcal{B}} \Big[\operatorname{Grad}\delta\boldsymbol{\varphi} : \partial^2_{\boldsymbol{FH}}\hat{\Psi}^* : \operatorname{Grad}\Delta(-\Phi) + \operatorname{Grad}\delta(-\Phi) : \partial^2_{\boldsymbol{HH}}\hat{\Psi}^* : \operatorname{Grad}\Delta(-\Phi)\Big] dV.$$

One easily observes the common structure of the mechanical and magnetic terms in (56), (57) and (58). Motivated by this observation one may write the variational principle (56) in the following *compact notation* form

$$I(\mathfrak{u}) := \int_{\mathcal{B}} \hat{\Psi}^*(\mathfrak{G}(\mathfrak{u}))\, dV - \int_{\partial\mathcal{B}_{\mathfrak{T}}} \bar{\mathfrak{T}} \cdot \mathfrak{u}\, dA \quad \longrightarrow \text{stat.} , \tag{60}$$

where we have introduced the *generalized primary variable vector* $\mathfrak{u} := [\boldsymbol{\varphi}, -\phi]^T$, the *generalized deformation gradient* $\mathfrak{G} := \operatorname{Grad}\mathfrak{u} = [\boldsymbol{F}, \boldsymbol{H}]^T$ and the *generalized prescribed traction vector* $\bar{\mathfrak{T}} := \big[\bar{\boldsymbol{t}}^{\,t}, -\bar{B}\big]^T$. The necessary condition for the stationarity of (60) can then similarly be written as

$$\delta I(\mathfrak{u}, \delta\mathfrak{u}) = \int_{\mathcal{B}} \partial_{\mathfrak{G}}\hat{\Psi}^* \cdot \operatorname{Grad}\delta\mathfrak{u}\, dV - \int_{\partial\mathcal{B}_{\mathfrak{T}}} \bar{\mathfrak{T}} \cdot \delta\mathfrak{u}\, dA \stackrel{!}{=} 0 . \tag{61}$$

The constitutive relations, which are needed for the evaluation of (61), have been specified in (55c). Denoting the generalized stress tensor by $\mathfrak{s} = \big[\boldsymbol{P}^t, -\boldsymbol{B}\big]^T$, these relations read $\mathfrak{s} = \partial_{\mathfrak{G}}\hat{\Psi}^*(\mathfrak{G})$. Finally, the compact notation equivalent of the linearized weak form (58), also substituting the increment expressions (59), is given by

$$\operatorname{Lin} G(\bar{\mathfrak{u}}, \delta\bar{\mathfrak{u}}, \Delta\mathfrak{u}) = G(\bar{\mathfrak{u}}, \delta\bar{\mathfrak{u}}) + \int_{\mathcal{B}} \Big[[\operatorname{Grad}\delta\mathfrak{u}]^T \cdot \partial^2_{\mathfrak{G}\mathfrak{G}}\hat{\Psi}^* \cdot \operatorname{Grad}\Delta\mathfrak{u}\Big] dV - \int_{\partial\mathcal{B}_{\mathfrak{T}}} \bar{\mathfrak{T}} \cdot \delta\mathfrak{u}\, dA. \tag{62}$$

4. Numerical Implementation of Finite Magnetomechanics

Since analytical solutions for the geometrically- and physically-nonlinear boundary value problems of finite magnetomechanics can be derived only for a limited number of special cases, computational methods must be employed in general. In this section a finite element model is proposed which allows the computation of approximate numerical solutions to the variational problem (60), described in Section 3.6.

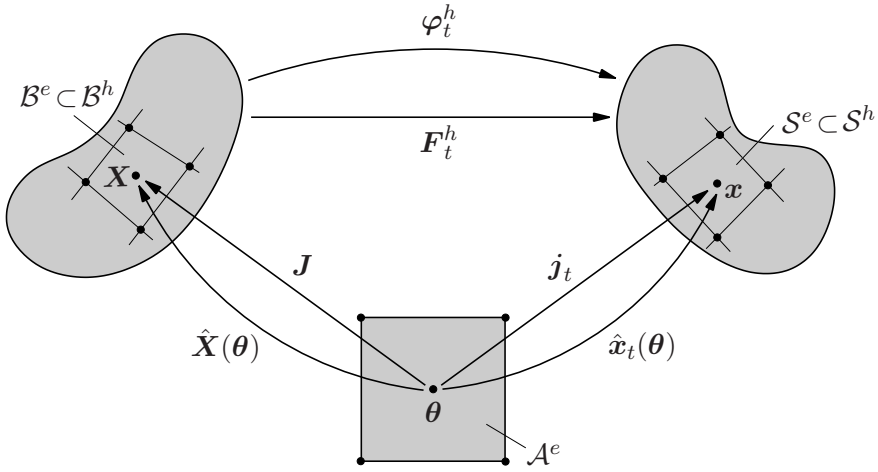

Figure 16: Isoparametric mappings between the element parameter space $\mathcal{A}^e$ and the associated finite elements $\mathcal{B}^e \subset \mathcal{B}^h$ and $\mathcal{S}^e \subset \mathcal{S}^h$ in the Lagrangian and Eulerian settings.

In the standard finite element approach the *spatial discretization* of the continuum body $\mathcal{B}$ is based on its approximate subdivision into a set of n_{el} finite elements $\mathcal{B}^e \subset \mathcal{B}^h$, such that

$$\mathcal{B} \approx \mathcal{B}^h = \bigcup_{e=1}^{n_{el}} \mathcal{B}^e \ , \tag{63}$$

where the symbol $\bigcup_{e=1}^{n_{el}}$ denotes the standard finite element assembly operator. One further defines a reference element $\mathcal{A}^e$ with local coordinates $\boldsymbol{\theta}$, as shown in Figure 16. The coordinates of the element in the material setting $\boldsymbol{X}^h \in \mathcal{B}^e$ and the spatial setting $\boldsymbol{x}^h \in \mathcal{S}^e$ are then described by the isoparametric *Lagrangian* and *Eulerian parameter maps*

$$\hat{\boldsymbol{X}} := \begin{cases} \mathcal{A}^e \to \mathcal{B}^e \subset \mathcal{B}^h \ , \\ \boldsymbol{\theta} \mapsto \boldsymbol{X}^h = \hat{\boldsymbol{X}}(\boldsymbol{\theta}) \end{cases} , \qquad \hat{\boldsymbol{x}}_t := \begin{cases} \mathcal{A}^e \to \mathcal{S}^e \subset \mathcal{S}^h \ , \\ \boldsymbol{\theta} \mapsto \boldsymbol{x}^h = \hat{\boldsymbol{x}}_t(\boldsymbol{\theta}) \end{cases} . \tag{64}$$

These mappings approximate the material and spatial coordinates on the basis of the standard expressions

$$\boldsymbol{X} \approx \boldsymbol{X}^h = \hat{\boldsymbol{X}}(\boldsymbol{\theta}) = \sum_{\alpha=1}^{n_{npe}} \hat{N}^\alpha(\boldsymbol{\theta}) \boldsymbol{D}^\alpha = \hat{\boldsymbol{N}}(\boldsymbol{\theta}) \boldsymbol{D} \ , \tag{65a}$$

$$\boldsymbol{x} \approx \boldsymbol{x}^h = \hat{\boldsymbol{x}}_t(\boldsymbol{\theta}) = \sum_{\alpha=1}^{n_{npe}} \hat{N}^\alpha(\boldsymbol{\theta}) \boldsymbol{d}_t^\alpha = \hat{\boldsymbol{N}}(\boldsymbol{\theta}) \boldsymbol{d}_t \ , \tag{65b}$$

where n_{npe}, denotes the number of nodes per element, $\hat{\boldsymbol{N}}$ represents the matrix of shape functions parameterized in the local coordinates $\boldsymbol{\theta} \in \mathcal{A}^e$ of the finite element parameter

space. The vectors $\boldsymbol{D} \in \mathbb{R}^{\dim \cdot n_{npe}}$ and $\boldsymbol{d}_t \in \mathbb{R}^{\dim \cdot n_{npe}}$, where $\dim \in \{1,2,3\}$ are the spatial dimensions of the considered problem, contain the discrete Lagrangian and Eulerian nodal positions of element $\mathcal{B}^e$ at time t, respectively. Based on the introduced approximate mappings and again referring to Figure 16, the deformation map can be expressed as

$$\boldsymbol{\varphi}_t^h(\boldsymbol{X}^h) := \hat{\boldsymbol{x}}_t \circ \hat{\boldsymbol{X}}^{-1} = \hat{\boldsymbol{x}}_t\big(\boldsymbol{\theta}(\boldsymbol{X}^h)\big) \ . \tag{66}$$

One may further define the gradients

$$\boldsymbol{J} := \partial_{\boldsymbol{\theta}} \hat{\boldsymbol{X}} = \partial_{\boldsymbol{\theta}} \Big[\sum_{\alpha=1}^{n_{npe}} \hat{N}^\alpha(\boldsymbol{\theta}) \boldsymbol{D}^\alpha \Big] = \sum_{\alpha=1}^{n_{npe}} \boldsymbol{D}^\alpha \otimes \partial_{\boldsymbol{\theta}} \hat{N}^\alpha(\boldsymbol{\theta}), \text{ with } J^A{}_i = \frac{\partial \hat{X}^A}{\partial \theta^i} = \sum_{\alpha=1}^{n_{npe}} \hat{N}^\alpha_{,i} (\boldsymbol{D}^\alpha)^A,$$

$$\boldsymbol{j}_t := \partial_{\boldsymbol{\theta}} \hat{\boldsymbol{x}} = \partial_{\boldsymbol{\theta}} \Big[\sum_{\alpha=1}^{n_{npe}} \hat{N}^\alpha(\boldsymbol{\theta}) \boldsymbol{d}_t^\alpha \Big] = \sum_{\alpha=1}^{n_{npe}} \boldsymbol{d}_t^\alpha \otimes \partial_{\boldsymbol{\theta}} \hat{N}^\alpha(\boldsymbol{\theta}), \text{ with } j^a{}_i = \frac{\partial \hat{x}^a}{\partial \theta^i} = \sum_{\alpha=1}^{n_{npe}} \hat{N}^\alpha_{,i} (\boldsymbol{d}_t^\alpha)^a.$$

Note that, based on the chain rule, the above mappings may be utilized to related derivatives in parameter space to derivatives in the reference and current configurations via

$$\operatorname{Grad} \hat{\boldsymbol{N}} = \boldsymbol{J}^{-T} \partial_{\boldsymbol{\theta}} \hat{\boldsymbol{N}} \ , \qquad \operatorname{grad} \hat{\boldsymbol{N}} = \boldsymbol{j}_t^{-T} \partial_{\boldsymbol{\theta}} \hat{\boldsymbol{N}} \ . \tag{67}$$

With these definitions at hand, the deformation gradient is approximated as

$$\boldsymbol{F}_t^h = \operatorname{Grad} \boldsymbol{\varphi}_t^h(\boldsymbol{X}^h) = \operatorname{Grad} \big[\hat{x}_t\big(\boldsymbol{\theta}(\boldsymbol{X}^h)\big) \big] = \partial_{\boldsymbol{\theta}} \hat{x}_t \, \partial_{\boldsymbol{X}^h} \boldsymbol{\theta} = \boldsymbol{j}_t \boldsymbol{J}^{-1} =: \hat{\boldsymbol{B}} \boldsymbol{d}_t \ . \tag{68}$$

The matrix $\hat{\boldsymbol{B}}(\boldsymbol{X}^h)$ contains the derivatives of the shape functions with respect to the Lagrangian coordinates $\boldsymbol{X}^h$.[12] Following the *isoparametric concept*, in which the geometry and the field variables are approximated over the element domain by the same set of shape functions, one can approximate the scalar magnetic potential, completely analogously to (65), as

$$-\Phi \approx -\Phi^h = \hat{\Phi}_t(\boldsymbol{\theta}) = \sum_{\alpha=1}^{n_{npe}} \hat{N}^\alpha(\boldsymbol{\theta}) (\boldsymbol{d}_t^\Phi)^\alpha = \hat{\boldsymbol{N}} \boldsymbol{d}_t^\Phi \ , \tag{70}$$

where the vector $\boldsymbol{d}_t^\Phi$ contains the (negative) magnetic potential value at the different nodes at time t.

Utilizing again the compact notation concept that was used for the concise representation of the variational problem (60), we introduce the *generalized nodal degree of freedom vector* $\mathfrak{d} \in \mathbb{R}^{N(\dim+1)}$, which contains the current nodal positions $\boldsymbol{d}_t$ and negative magnetic potential values $\boldsymbol{d}_t^\Phi$ at time t at all N nodes of the mesh in an assembled format. Note that we have dropped the superscript t. It is henceforth implied that all discrete variables are evaluated at the current time t, or more accurately at the discrete time t_{n+1} at the end of the current time interval. The *discrete generalized primary variable vector* and *discrete generalized deformation gradient* are then computed from the relations

$$\mathfrak{u}^h = \mathfrak{N} \mathfrak{d} \ , \qquad \mathfrak{G}^h = \operatorname{Grad}\big[\mathfrak{u}^h\big] = \mathfrak{B} \mathfrak{d} \ , \tag{71}$$

[12] The compact notation matrix relation $\boldsymbol{F}_t^h = \hat{\boldsymbol{B}} \boldsymbol{d}_t$ is to be interpreted in the sense that

$$F^a{}_A = \sum_{\alpha=1}^{n_{npe}} \frac{\partial \hat{N}^\alpha}{\partial \theta^i} (\boldsymbol{d}_t^\alpha)^a (\boldsymbol{J}^{-1})^i{}_A = \sum_{\alpha=1}^{n_{npe}} (\boldsymbol{d}_t^\alpha)^a \frac{\partial \hat{N}^\alpha}{\partial \boldsymbol{X}^A} = \sum_{\alpha=1}^{n_{npe}} (\boldsymbol{d}_t^\alpha)^a \hat{B}^\alpha{}_A \ . \tag{69}$$

where $\mathfrak{N}$ and $\mathfrak{B}$ are the *generalized shape function* and their associated *gradient matrices*. By defining the analogous approximations $\delta\mathfrak{u}^h = \mathfrak{N}\,\delta\mathfrak{d}$ and $\mathrm{Grad}\big[\delta\mathfrak{u}^h\big] = \mathfrak{B}\,\delta\mathfrak{d}$ and substituting into (61), one obtains the discrete equivalent of the necessary condition for stationarity in the continuous setting as

$$\delta I^h = \int_{\mathcal{B}} \mathfrak{s}^h \cdot \mathfrak{B}^T \delta\mathfrak{d}\; dV - \int_{\partial\mathcal{B}_{\bar{\mathfrak{T}}}} \bar{\mathfrak{T}} \cdot \mathfrak{N}^T \delta\mathfrak{d}\; dA =: I^h_{,\mathfrak{d}} \cdot \delta\mathfrak{d} = 0 \;, \tag{72}$$

where the *finite element residual vector* has been defined as

$$\mathfrak{R} := I^h_{,\mathfrak{d}}(\mathfrak{d}) = \int_{\mathcal{B}} \mathfrak{B}^T \mathfrak{s}^h\; dV - \int_{\partial\mathcal{B}_{\bar{\mathfrak{T}}}} \mathfrak{N}^T \bar{\mathfrak{T}}\; dA = \boldsymbol{0} \;. \tag{73}$$

Equation (73) represents a nonlinear algebraic system for the determination of the generalized displacement vector $\mathfrak{d}$ of the coupled magneto-mechanical problem. To find the roots of the nonlinear problem $\mathfrak{R} = I^h_{,\mathfrak{d}}(\mathfrak{d}) = \boldsymbol{0}$, an iterative solution procedure must be employed. Following a standard *Newton-Raphson scheme*, one obtains the following update relation for the nodal degree of freedom vector

$$\mathfrak{d} \Leftarrow \mathfrak{d} - \big[I^h_{,\mathfrak{d}\mathfrak{d}}(\mathfrak{d})\big]^{-1} I^h_{,\mathfrak{d}}(\mathfrak{d}) = \mathfrak{d} - \mathfrak{K}^{-1}\mathfrak{R} \;. \tag{74}$$

The iteration procedure is terminated if the norm of the residual falls below as certain tolerance, i.e. $\|\mathfrak{R}\| < tol$. In the preceding expressions we have utilized the definitions of the *finite element tangent matrix*

$$\mathfrak{K} := I^h_{,\mathfrak{d}\mathfrak{d}}(\mathfrak{d}) = \int_{\mathcal{B}} \mathfrak{B}^T \mathfrak{C}^h \mathfrak{B}\; dV \;, \tag{75}$$

where we have assumed dead loads, and the *discrete generalized stresses* and *discrete coupled moduli*

$$\mathfrak{s}^h := \partial_{\mathfrak{G}^h} \hat{\psi}^*(\mathfrak{B}\mathfrak{d}) \;, \qquad \mathfrak{C}^h := \partial^2_{\mathfrak{G}^h \mathfrak{G}^h} \hat{\psi}^*(\mathfrak{B}\mathfrak{d}) \;. \tag{76}$$

It must be emphasized that due to the chosen variational formulation the tangent matrix $\mathfrak{K}$ is automatically *symmetric*, and consequently solvers for symmetric linear systems of equations can be employed in the iterative solution procedure of the nonlinear problem.

5. Constitutive Models of Finite Magnetoelasticity

In this section three specific constitutive models for finite magnetostriction are proposed: i) *an extended compressible Neo-Hookean model*, ii) *an anisotropic extension of the first model* and iii) *an isotropic model with saturation of the magnetomechanical coupling effect*. These model are presented in a coordinate-independent formulation, which is based on the framework of invariant theory, which shall be introduced next.

5.1. Invariant Theory of Isotropic Tensor Functions

According to *representation theorems for isotropic tensor functions* (see for example Boehler [1]), scalar-valued isotropic functions Ψ^* of two symmetric second order tensor arguments $\boldsymbol{C}$ and $\boldsymbol{H}\otimes\boldsymbol{H}$, i.e. $\hat{\Psi}^*(\boldsymbol{C},\boldsymbol{H}\otimes\boldsymbol{H})$, allow representations based on the irreducible polynomial basis given by the combined set of mechanical, magnetic and coupling invariants

$$\begin{aligned}\mathcal{I} := \{I_1,\dots,I_6\} = \big\{&\mathrm{tr}[\boldsymbol{C}]_{\boldsymbol{G}^{-1}}, \mathrm{tr}\big[\boldsymbol{C}^2\big]_{\boldsymbol{G}^{-1}}, \det[\boldsymbol{C}]_{\boldsymbol{G}^{-1}}, \mathrm{tr}[\boldsymbol{H}\otimes\boldsymbol{H}]_{\boldsymbol{G}^{-1}},\\ &\mathrm{tr}[\boldsymbol{C}(\boldsymbol{H}\otimes\boldsymbol{H})]_{\boldsymbol{G}^{-1}}, \mathrm{tr}\big[\boldsymbol{C}^2(\boldsymbol{H}\otimes\boldsymbol{H})\big]_{\boldsymbol{G}^{-1}}\big\}\ ,\end{aligned} \tag{77}$$

where $\det[\boldsymbol{C}]_{\boldsymbol{G}^{-1}}$ has replaced the invariant $\mathrm{tr}\big[\boldsymbol{C}^3\big]_{\boldsymbol{G}^{-1}}$ for convenience. This is possible since, by means of the *Cayley-Hamilton theorem*, one can express $\det[\boldsymbol{C}]_{\boldsymbol{G}^{-1}}$ as a polynomial of the invariants $\mathrm{tr}[\boldsymbol{C}]_{\boldsymbol{G}^{-1}}$, $\mathrm{tr}\big[\boldsymbol{C}^2\big]_{\boldsymbol{G}^{-1}}$ and $\mathrm{tr}\big[\boldsymbol{C}^3\big]_{\boldsymbol{G}^{-1}}$.

In combination with the discussion of thermodynamic consistency in Section 3.4, the objective free energy-enthalpy for a general isotropic hyperelastic magnetic solid can be written as

$$\hat{\Psi}^*(\boldsymbol{C},\boldsymbol{H}\otimes\boldsymbol{H}) = \hat{\Psi}^*(\mathcal{I})\ . \tag{78}$$

Constitutive equations of the general form (78) thus a priori satisfy the material symmetry constraint (52) on the reduced form of the free energy-enthalpy function for isotropic materials where $\mathcal{G}\equiv\mathcal{SO}(3)$.

From the general constitutive relations (55c), one then obtains the constitutive relations specified for general isotropic hyperelastic magnetic solids in terms of the total first Piola-Kirchhoff stresses

$$\begin{aligned}\boldsymbol{g}\boldsymbol{P}^t &= \partial_{\boldsymbol{F}}\hat{\Psi}^*(\boldsymbol{C},\boldsymbol{H}) = 2\,\boldsymbol{g}\boldsymbol{F}\partial_{\boldsymbol{C}}\hat{\Psi}^*\\ &= 2\,\boldsymbol{g}\boldsymbol{F}\Big[\hat{\Psi}^*_{,I_1}\,\partial_{\boldsymbol{C}}I_1 + \hat{\Psi}^*_{,I_2}\,\partial_{\boldsymbol{C}}I_2 + \hat{\Psi}^*_{,I_3}\,\partial_{\boldsymbol{C}}I_3 + \hat{\Psi}^*_{,I4}\,\partial_{\boldsymbol{C}}I_4 + \hat{\Psi}^*_{,I_5}\,\partial_{\boldsymbol{C}}I_5 + \hat{\Psi}^*_{,I_6}\,\partial_{\boldsymbol{C}}I_6\Big]\\ &= 2\,\boldsymbol{g}\boldsymbol{F}\Big[\hat{\Psi}^*_{,I_1}\boldsymbol{G}^{-1} + 2\,\hat{\Psi}^*_{,I_2}\boldsymbol{G}^{-1}\boldsymbol{C}\boldsymbol{G}^{-1} + I_3\,\hat{\Psi}^*_{,I_3}\boldsymbol{C}^{-1} + \hat{\Psi}^*_{,I_5}\boldsymbol{G}^{-1}\boldsymbol{H}\otimes\boldsymbol{G}^{-1}\boldsymbol{H}\\ &\qquad +2\,\hat{\Psi}^*_{,I6}\,\mathrm{sym}\big[\boldsymbol{G}^{-1}\boldsymbol{H}\otimes\boldsymbol{G}^{-1}\boldsymbol{C}\boldsymbol{G}^{-1}\boldsymbol{H}\big]\Big]\ ,\end{aligned} \tag{79}$$

where the last step was based on the calculation of the partial derivatives of the invariants (77) with respect to the deformation gradient. Similarly, for the Lagrangian magnetic induction one finds

$$\begin{aligned}\boldsymbol{B} &= -\partial_{\boldsymbol{H}}\hat{\Psi}^*(\boldsymbol{C},\boldsymbol{H})\\ &= -\partial_{I_1}\hat{\Psi}^*\partial_{\boldsymbol{H}}I_1 - \partial_{I_2}\hat{\Psi}^*\partial_{\boldsymbol{H}}I_2 - \partial_{I_3}\hat{\Psi}^*\partial_{\boldsymbol{H}}I_3 - \partial_{I_4}\hat{\Psi}^*\partial_{\boldsymbol{H}}I_4 - \partial_{I_5}\hat{\Psi}^*\partial_{\boldsymbol{H}}I_5 - \partial_{I_6}\hat{\Psi}^*\partial_{\boldsymbol{H}}I_6\\ &= -2\left[\hat{\Psi}^*_{,I_4}\boldsymbol{G}^{-1} + \hat{\Psi}^*_{,I_5}\boldsymbol{G}^{-1}\boldsymbol{C}\boldsymbol{G}^{-1} + \hat{\Psi}^*_{,I_6}\boldsymbol{G}^{-1}\boldsymbol{C}^2\boldsymbol{G}^{-1}\right]\boldsymbol{H}\ . \end{aligned} \tag{80}$$

5.2. An Extended Compressible Neo-Hookean Model

As a first example we consider the extension of a classical Neo-Hooke material to incorporated magnetizability of the material and magnetomechanical coupling effects. To this end the magnetic invariant I_4 is included in the free energy-enthalpy function to model the magnetic behavior and in variant I_5 to capture the macroscopic influence of the micro-scale magnetomechanical particle-matrix interactions in a phenomenological sense. Following the decomposition of the amended free energy-enthalpy function into material and a free space contributions (40), its specific form for the extended compressible Neo-Hookean-type model of finite magnetostriction is proposed as

$$\begin{aligned}\Psi^* &= \hat{\Psi}^*(\boldsymbol{F},\boldsymbol{H}) = \hat{\psi}^*(\boldsymbol{F},\boldsymbol{H}) + \hat{\psi}^{*,free}(\boldsymbol{H})\\ &= \frac{\mu}{2}(I_1 - \ln[I_3] - 3) + \frac{\lambda}{8}(\ln[I_3])^2 + c_1 I_4 + c_2 I_5 - \frac{\mu_0}{2} I_3^{-\frac{1}{2}}\left[I_6 - I_1 I_5 + \frac{1}{2}\left(I_1^2 - I_2\right) I_4\right]\\ &= \frac{\mu}{2}(\boldsymbol{G}^{-1}\boldsymbol{C} - 3) - \mu\ln[J] + \frac{\lambda}{2}(\ln[J])^2 + \left(c_1\boldsymbol{G}^{-1} + c_2\boldsymbol{G}^{-1}\boldsymbol{C}\boldsymbol{G}^{-1}\right) : (\boldsymbol{H}\otimes\boldsymbol{H})\\ &\quad -\frac{1}{2}\mu_0 J\boldsymbol{C}^{-1} : (\boldsymbol{H}\otimes\boldsymbol{H})\ , \end{aligned} \tag{81}$$

where μ and λ are the *Lamé parameters* (μ is also called the *shear modulus)*, c_1 is the *magnetic coefficient* related to the permeability of the material and c_2 is the *magnetomechanical coupling coefficient*.

By evaluating the partial derivatives of (81) with respect to the invariants and substituting into (79) and (80) one then obtains the specific constitutive equations

$$\begin{aligned}\boldsymbol{g}\boldsymbol{P}^t = \quad \partial_{\boldsymbol{F}}\Psi^* &= \mu\boldsymbol{F}\boldsymbol{G}^{-1} + (\lambda\ln[J] - \mu)\,\boldsymbol{F}^{-T}\boldsymbol{G} + 2c_2\boldsymbol{F}\boldsymbol{G}^{-1}\boldsymbol{H}\otimes\boldsymbol{G}^{-1}\boldsymbol{H}\\ &\quad +\mu_0 J(\boldsymbol{F}^{-T}\boldsymbol{H}\otimes\boldsymbol{C}^{-1}\boldsymbol{H}) - \frac{\mu_0}{2}J\left[\boldsymbol{C}^{-1} : (\boldsymbol{H}\otimes\boldsymbol{H})\right]\boldsymbol{F}^{-T} \end{aligned} \tag{82a}$$

$$\boldsymbol{B} = -\partial_{\boldsymbol{H}}\Psi^* = -2c_1\boldsymbol{G}^{-1}\boldsymbol{H} - 2c_2\boldsymbol{G}^{-1}\boldsymbol{C}\boldsymbol{G}^{-1}\boldsymbol{H} + \mu_0 J\boldsymbol{C}^{-1}\boldsymbol{H}\ . \tag{82b}$$

It must be pointed out that typically the free space contributions to the free energy-enthalpy function are considered small and are therefore neglected in computations. In some cases, however, where for example the magnetostatic attraction of the magnetized iron particles on the microscale is to be modeled directly, free space terms are essential (see discussion in Kiefer, Rosato & Miehe [22]).

5.3. An Anisotropic Compressible Extended Neo-Hookean Model

As discussed in Section 2, some magnetorheological elastomers have the magnetic particles aligned in a preferred direction. In order to take into account this anisotropy,

we use the standard method of introducing a structural tensor $\bar{\boldsymbol{M}} = \boldsymbol{a} \otimes \boldsymbol{a}$ where $\boldsymbol{a}$ is the preferred direction. Thus we make use of an *isotropic free energy function with an extended list of arguments* to model isotropy.

$$\boldsymbol{\mathcal{I}} := \{I_1, .., I_{11}\} \ .$$

That is, in addition to the six invariants needed as a polynomial basis for the free energy function for an isotropic material, we have,

$$\begin{array}{rclrclrcl} I_7 &=& \mathrm{tr}\big[(\boldsymbol{H}\otimes\boldsymbol{H})\boldsymbol{C}\bar{\boldsymbol{M}}\big]_{\boldsymbol{G}^{-1}}, & I_8 &=& \mathrm{tr}\big[(\boldsymbol{H}\otimes\boldsymbol{H})\boldsymbol{C}^2\bar{\boldsymbol{M}}\big]_{\boldsymbol{G}^{-1}}, & I_9 &=& \mathrm{tr}\big[\boldsymbol{C}\bar{\boldsymbol{M}}\big]_{\boldsymbol{G}^{-1}} \\ I_{10} &=& \mathrm{tr}\big[\boldsymbol{C}^2\bar{\boldsymbol{M}}\big]_{\boldsymbol{G}^{-1}}, & I_{11} &=& \mathrm{tr}[\boldsymbol{H}\otimes\boldsymbol{a}]_{\boldsymbol{G}^{-1}} \ . \end{array}$$

For simplicity, we take no dependence of Ψ on $I_8....I_{11}$

$$\Psi = \frac{\mu}{2}(I_1 - 3) - \frac{\mu}{2}\ln[I_3] + \frac{\lambda}{4}(\ln[I_3])^2 + c_1 I_4 + c_2 I_5 + c_3 I_7 \ . \tag{83}$$

Accordingly, we have the following derived quantities

$$\begin{aligned} \boldsymbol{g}\boldsymbol{P}^t = \quad \partial_{\boldsymbol{F}}\Psi &= \mu\boldsymbol{F}\boldsymbol{G}^{-1} - \mu\boldsymbol{F}^{-T}\boldsymbol{G} + \lambda\ln[J]\,\boldsymbol{F}^{-T}\boldsymbol{G} + 2c_2\boldsymbol{F}\boldsymbol{G}^{-1}\boldsymbol{H}\otimes\boldsymbol{G}^{-1}\boldsymbol{H} \\ &\quad + c_3\boldsymbol{F}\boldsymbol{G}^{-1}\,\mathrm{sym}\big[\boldsymbol{H}\otimes\bar{\boldsymbol{M}}\boldsymbol{H}\big], \end{aligned} \tag{84a}$$

$$\begin{aligned} \boldsymbol{B} = -\,\partial_{\boldsymbol{H}}\Psi &= -2c_1\boldsymbol{G}^{-1}\boldsymbol{H} - 2c_2\boldsymbol{G}^{-1}\boldsymbol{C}\boldsymbol{G}^{-1}\boldsymbol{H} \\ &\quad - c_3\boldsymbol{G}^{-1}\left[(\boldsymbol{C}\bar{\boldsymbol{M}})^T\boldsymbol{H} + \boldsymbol{C}\bar{\boldsymbol{M}}\boldsymbol{H}\right] \ . \end{aligned} \tag{84b}$$

Thus, in addition to the material parameters in the isotropic case, we have an additional material parameter c_3 which may be viewed as a measure of the *coupling in the preferred direction.*

5.4. An Isotropic Model with Saturation of the Magnetomechanical Coupling Effect

Tests done on magnetorheological elastomers show a 'saturation effect'. This is attributed to the existence of a saturation value of magnetization of the embedded iron particles. With increasing applied field $\boldsymbol{H}$, the magnetization of these particles increases up to a certain saturation value m_{sat}. After this point, any increase in applied field does not have any further stiffening effect on the material. In order to take the above effect into account, we modify the free energy function to

$$\Psi^* = \frac{1}{k}\left[\mu_0 + \mu_{sat}\tanh(\bar{I}_4^n)\right]\left[\frac{(I_1-1)^k}{2^k} - 1\right] - \frac{\mu_0}{2}\ln[I_3] + \frac{\lambda}{4}(\ln[I_3])^2 + f(\bar{I}_4) \ , \tag{85}$$

where we have used a dimensionless form of I_4 as,

$$\bar{I}_4 = I_4/\xi \ . \tag{86}$$

Here $f(\bar{I}_4)$ is physically interpreted as the energy in the undeformed configuration (in which there is a residual stress due to the presence of the magnetic field). It is convenient to assume a form for f such that $f'(\bar{I}_4)$ is given by

$$f'(\bar{I}_4) = -\xi\gamma_0\bar{I}_4^{n-1}\mathrm{sech}^2(\bar{I}_4^n) + \xi\delta_0\tanh(\bar{I}_4^2) - \xi\varepsilon_0 \ . \tag{87}$$

The reason for the particular form of f' is so that, like shear modulus, we also have the the magnetic induction $\boldsymbol{B}$ reaching a maximum value independent of $\boldsymbol{H}$. The above free energy function give us the resulting constitutive equations as

$$\begin{aligned} \boldsymbol{g}\boldsymbol{P}^t = \quad \partial_{\boldsymbol{F}}\Psi^* &= \left[\mu_0 + \mu_{sat}\tanh(\bar{I}_4^n)\right]\left(\frac{I_1-1}{2}\right)^{k-1}\boldsymbol{F}\boldsymbol{G}^{-1} \\ &\quad -\mu\boldsymbol{F}^{-T} + \lambda\ln[J]\,\boldsymbol{F}^{-T}\boldsymbol{G}\ , \end{aligned} \tag{88a}$$

$$\begin{aligned} \boldsymbol{B} = -\,\partial_{\boldsymbol{H}}\Psi^* &= -2\bar{I}_4^{n-1}\mathrm{sech}^2(\bar{I}_4^n)\left\{\frac{n\mu_{sat}}{k\xi}\left[\left(\frac{I_1-1}{2}\right)^k - 1\right] + 2\gamma_0\right\}\boldsymbol{G}^{-1}\boldsymbol{H} \\ &\quad -2\delta_0\tanh(\bar{I}_4^2)\,\boldsymbol{G}^{-1}\boldsymbol{H} + 2\varepsilon_0\,\boldsymbol{G}^{-1}\boldsymbol{H}\ . \end{aligned} \tag{88b}$$

In this model, μ_0 is the shear modulus of the material at *zero magnetic field* and μ_{sat} is the maximum increase in shear modulus (due to magnetic field). The parameter ε_0 is now the coefficient related to the magnetic permeability of free space while δ_0 and γ_0 are additional parameters related to the purely magnetic part and describe the *material's* magnetic response. The remaining parameter ξ, is a scaling factor related to the coupling of magnetic and mechanical response.

With these expressions above we can code the different material models to obtain a finite element solution. However, before we do that, we will test the material models with some driver tests. The results of these tests are the first part of the next section.

6. Numerical Results

6.1. Driver Tests

To test the proposed models, we would like to see the response to some simple deformation driven tests at the *material point level*. To achieve this, we present below, the *driver algorithms* used to evaluate the materials response to some simple deformation processes. The results of the driver tests should help us analyze the results of boundary value problems presented later in this chapter.

6.1.1. Simple Shear Driver. It is of interest to see how the response of the model to *shear deformation* is altered by the magnetic field. To observe this we need to apply a shear deformation at different magnetic fields and look at the stress response. We can then plot shear stress vs. shear strain for these different magnetic fields as shown later. In a cartesian coordinate system, given the shear deformation

$$F_{n+1} = F^1{}_2(t_{n+1}) \tag{89}$$

at constant magnetic field in y- direction,

$$H_{n+1} = H_2 \tag{90}$$

we want the equivalent stress component

$$P_{n+1} = P^{12}(\boldsymbol{F}_{n+1}, \boldsymbol{H}_{n+1}) \tag{91}$$

The above are scalar quantities but our material law gives us tensorial quantities. The key step here, is the partitioning of the strain tensor as follows

$$\boldsymbol{F}_{n+1} = F_{n+1}\boldsymbol{e}_1 \otimes \boldsymbol{E}^2 + \bar{\boldsymbol{F}}_{n+1} \tag{92a}$$

$$\boldsymbol{H}_{n+1} = H_{n+1}\boldsymbol{E}^2 + \bar{\boldsymbol{H}}_{n+1} \tag{92b}$$

where, in the present case of shear deformation and constant reference magnetic field,

$$\bar{\boldsymbol{F}}_{n+1} = \boldsymbol{1} \tag{93a}$$

and

$$\bar{\boldsymbol{H}}_{n+1} = \boldsymbol{0} \tag{93b}$$

Using $\boldsymbol{F}_{n+1}$ as above, in the constitutive model, we obtain $\boldsymbol{P}_{n+1}$. Thus we are now able to determine the response of the model to shear deformation. The above algorithm is concisely presented in Box 2.

Using the driver, we obtain the plots of shear stress vs shear strain for the different models that have been proposed here.

6.1.1.1. Extended Isotropic Neo-Hookean Material Model. For this model, we plot the shear stress vs. shear strain ie. P^{12} vs $F^1{}_2$ for different magnetic field strengths, in Figure 17(a). By observing that the slopes of the stress-strain graphs increases with increasing magnetic fields, one can conclude that the response of the material becomes stiffer at higher field strengths. Thus, this model captures *Feature 1* and *Feature 2* stated

1. Given $F_{n+1} = F^1{}_2(t_{n+1})$ and $\boldsymbol{H}_{n+1} = H_2\boldsymbol{E}^2$ (constant).Set

$$\bar{\boldsymbol{F}}_{n+1} = \bar{\boldsymbol{F}}_n = \boldsymbol{1}$$

2. Calculate the total deformation as

$$\boldsymbol{F}_{n+1} = F_{n+1}\boldsymbol{e}_1 \otimes \boldsymbol{E}^2 + \bar{\boldsymbol{F}}_{n+1}$$

3. Calculate the algorithmic stresses from the material routine

$$\boldsymbol{P}^t_{n+1} = \hat{\boldsymbol{P}}^t(\boldsymbol{F}_{n+1}, \boldsymbol{H}_{n+1})$$

and go back to 1. for next time step.

Box 2: Driver algorithm for simple shear.

Table 1: Material Parameters for *Isotropic Neo-Hookean model*.

$\kappa = 4.0 \times 10^3\,\mathrm{N/mm^2}$	$c_1 =$ - $2.5 \times 10^{-6}\,\mathrm{N/A\,mm}$
$\mu = 1.8\,\mathrm{N/mm^2}$	$c_2 = 5.0 \times 10^{-2}\,\mathrm{N/A\,mm}$

in Section 1, i.e. the material is Neo-Hookean with increasingly stiffer response for higher magnetic fields.

However, the results of the driver also bring out the main drawback of the model- the model gives a *monotonically increasing* stiffer response with magnetic field which implies that *Feature 3*, i.e. saturation of the shear modulus, is not captured. This can be verified by plotting shear modulus (G) vs. magnetic field, which has been reported for this model in Figure 17(b). The material parameters used in the simulation are stated in Table 1.

6.1.1.2. Transversely-Isotropic Material Model. Similarly, the results of the shear test driver on the *transversely-isotropic* model, are displayed in Figure 18 and Figure 19. In the case of the transversely-isotropic model, the model exhibits Neo-Hookean

Table 2: Material Parameters for *transversely-isotropic model*.

$\kappa = 4.0 \times 10^3\,\mathrm{N/mm^2}$	$c_2 = 0.0\,\mathrm{N/A\,mm}$
$\mu = 1.8\,\mathrm{N/mm^2}$	$c_3 = 5.0 \times 10^{-2}\,\mathrm{N/A\,mm}$
$c_1 = -2.5 \times 10^{-6}\,\mathrm{N/A\,mm}$	

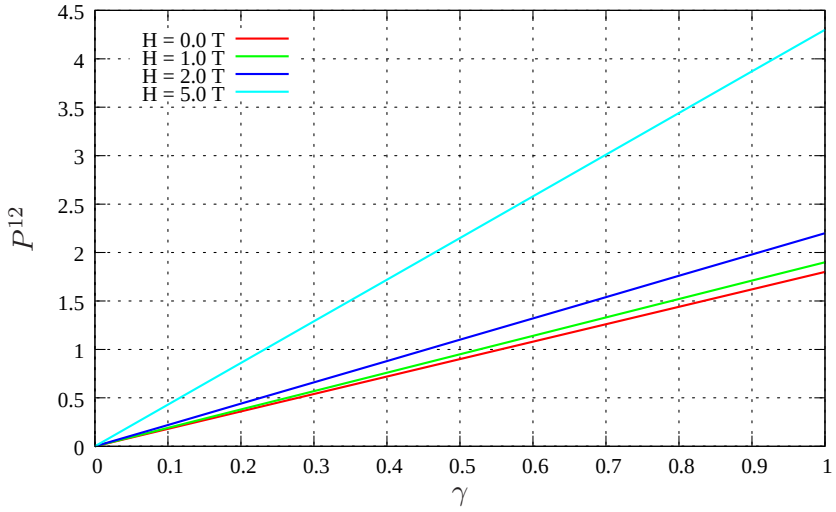

(a) Shear stress vs. shear strain at varying $\boldsymbol{H}$

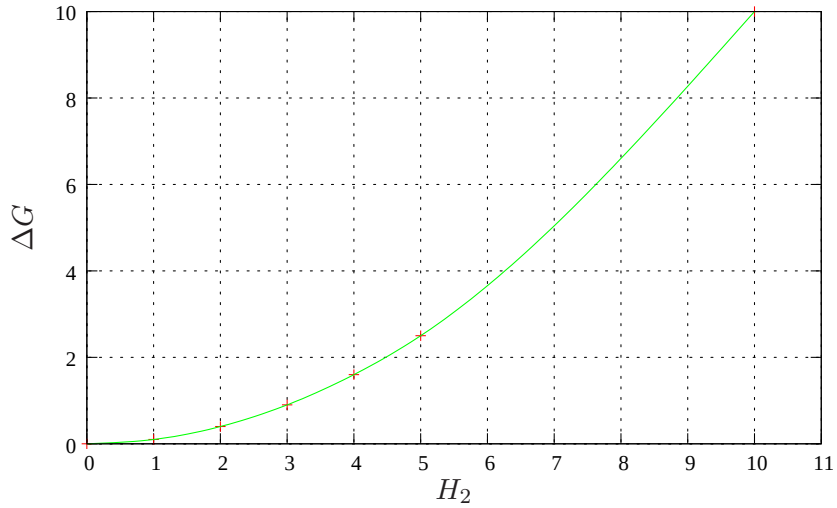

(b) Shear modulus vs applied $\boldsymbol{H}$

Figure 17: Simple shear of isotropic material model

behavior when the chains are aligned *perpendicular* to the magnetic field with the stress strain curves in different magnetic fields *falling on top of each other* (i.e. no effect of magnetic field on shear modulus G). However, when the chains are aligned *in the direction* of the magnetic field, the coupled behavior is 'switched on' and the material stiffens with increasing field strength. This is the desired response of the model since this coincides with experimental observations in [31]. The material parameters for the simulation are displayed in Table 2.

6.1.1.3. Saturation Type Material Model. The Isotropic Neo-Hookean model above, has the drawback that the stiffening effect monotonically increases with applied magnetic field strength whereas, in reality, it should approach a *saturation value*. In order to overcome this we have introduced the *Saturation type model*. We now use the driver to show the properties of this new model. The stress-strain plot is shown in Figure 20. It is seen that the shear modulus reaches a saturation value as the magnetic field is increased beyond a certain value. Thus this model successfully captures all the features i.e. *Features 1,2* and *3* that we stated in Section 2 for the materials with isotropic distribution of iron

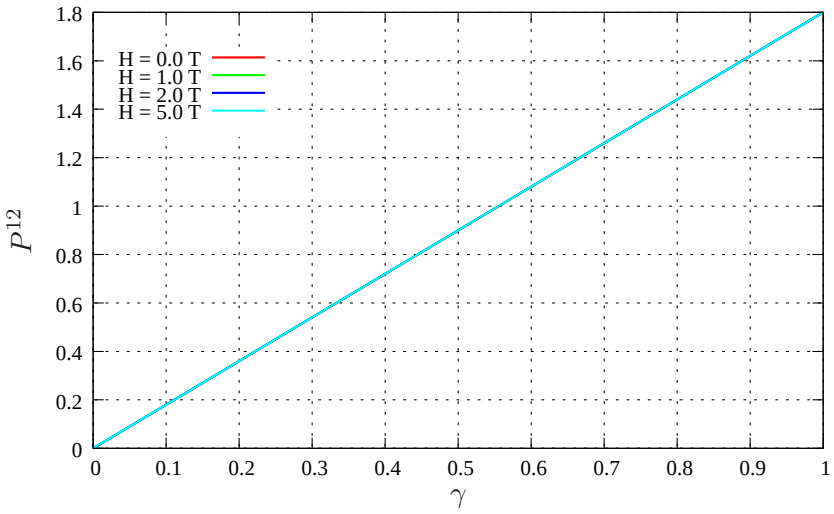

Figure 18: Simple shear of transversely-isotropic material model with $\boldsymbol{H}$ perpendicular to preferred direction

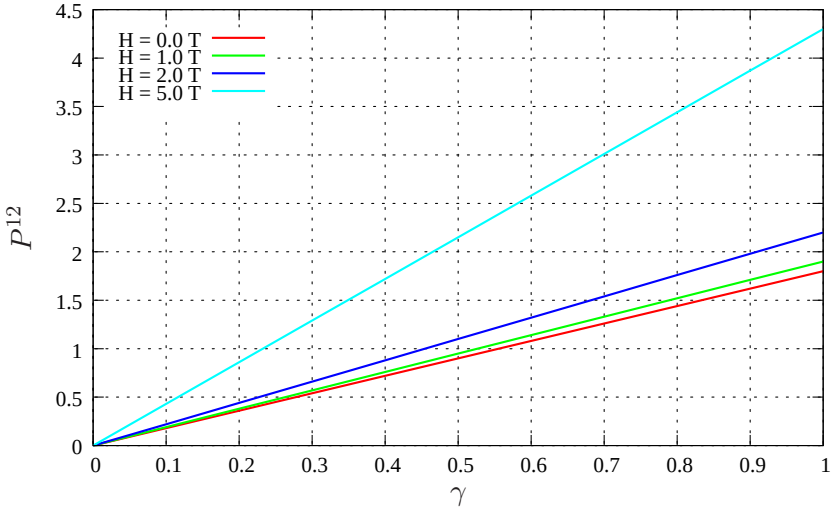

Figure 19: Simple shear of transversely-isotropic material model with $\boldsymbol{H}$ parallel to preferred direction

particles in the matrix i.e., in addition to the stiffening response, we also capture the saturation of the shear modulus with increasing magnetic field. The material parameters used for the simulation are listed in Table 3.

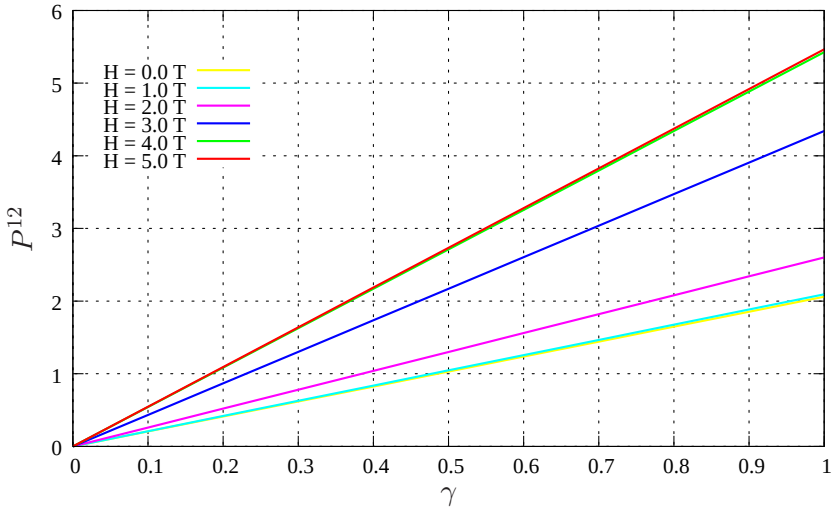

(a) Shear stress vs. shear strain at varying $\boldsymbol{H}$

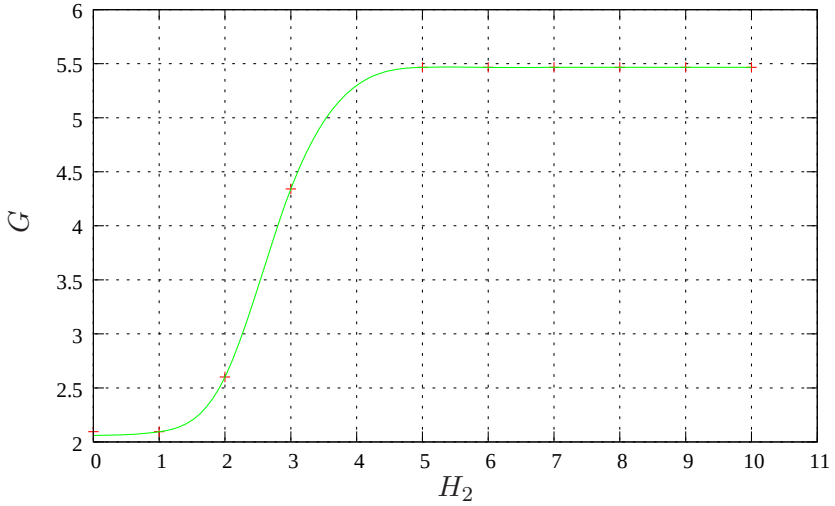

(b) Shear modulus vs applied $\boldsymbol{H}$

Figure 20: Simple shear of *Saturation type material model*

Table 3: Material Parameters for *Saturation type model.*

α_0	=	$2.06\,\mathrm{N/mm^2}$	ε_0	=	$6.2857 \times 10^{-7}\,\mathrm{N/A^2}$
β_0	=	$3.41\,\mathrm{N/mm^2}$	ξ	=	$10.0\,\mathrm{kA^2/m^2}$
γ_0	=	$9.49 \times 10^{-8}\,\mathrm{N/A^2}$	k	=	0.75
δ_0	=	$5.0 \times 10^{-7}\,\mathrm{N/A^2}$	n	=	2

6.1.2. Uniaxial Tension Test Driver. Another test of interest is a uniaxial test in constant magnetic field in which the stress state is one dimensional. Since this is deformation driven, the material is stretched along one direction, say the y-direction, and the other components of $\boldsymbol{F}$ are adjusted so as to allow a 1-D stress state

Clearly this requires an iterative procedure and is achieved as follows. Once more, working in a cartesian coordinate system, given the axial deformation

$$F_{n+1} = F^1{}_1(t_{n+1}) \tag{94}$$

the axial component of the stress

$$P_{n+1} = P^{11}(t_{n+1}) \tag{95}$$

is desired. We have the following partitions as

$$\boldsymbol{F}_{n+1} = F_{n+1}\boldsymbol{e}_1 \otimes \boldsymbol{E}^1 + \bar{\boldsymbol{F}}_{n+1} \tag{96a}$$

$$\boldsymbol{H}_{n+1} = H_{n+1}\boldsymbol{E}^1 + \bar{\boldsymbol{H}}_{n+1} \tag{96b}$$

$$\boldsymbol{P}_{n+1} = P_{n+1}\boldsymbol{e}_1 \otimes \boldsymbol{E}_1 + \bar{\boldsymbol{P}}_{n+1} \tag{96c}$$

In this case, H_{n+1} is a constant since we want to see the response in constant magnetic field. Now with $\boldsymbol{F}$ and $\boldsymbol{H}$ we call the material subroutine and obtain the stress and moduli. For a 1-D stress state, we should satisfy

$$\boldsymbol{R}_{n+1} := \bar{\boldsymbol{P}}_{n+1} = \boldsymbol{0} \tag{97}$$

We have to solve the following equation

$$\boldsymbol{R}_{n+1} + \Delta\boldsymbol{R}_{n+1} = \bar{\boldsymbol{P}}_{n+1} + \bar{\mathbb{A}}_{n+1} : \Delta\bar{\boldsymbol{F}}_{n+1} = \boldsymbol{0} \tag{98}$$

where $\bar{\mathbb{A}}_{n+1} := \partial\bar{\boldsymbol{F}}_{n+1}/\partial\bar{\boldsymbol{P}}_{n+1}$ is the partition of the moduli associated with $\bar{\boldsymbol{P}}_{n+1}$. This gives us the update for $\bar{\boldsymbol{F}}_{n+1}$ as follows:

$$\bar{\boldsymbol{F}}_{n+1} \Leftarrow \bar{\boldsymbol{F}}_{n+1} + \Delta\bar{\boldsymbol{F}}_{n+1} = \bar{\boldsymbol{F}}_{n+1} + \bar{\mathbb{A}}^{-1}_{n+1} : \bar{\boldsymbol{P}}_{n+1} \tag{99}$$

In every iteration step the material routine is called until the convergence criteria is satisfied ie.

$$\|\boldsymbol{R}_{n+1}\| \leq tol \tag{100}$$

The algorithm is concisely presented in Box 3 The results of the uniaxial tension test driver for the different models are presented below.

6.1.2.1. Extended Isotropic Neo-Hookean Material Model. Figure 21 is the plot of P^{22} vs $F^2{}_2$ for this model. The values of bulk and shear modulus are 10.0N/mm^2 and 5.0N/mm^2 respectively, while the values of c_1 and c_2 are the same as before. It is seen that the stress-strain plots have higher slopes for higher magnetic fields which is what is expected. The same explanations as stated in the shear driver tests hold here- increasing magnetic field leads to increasingly stiffer response.

1. Given $F_{n+1} = F_{11}(t_{n+1})$ and $\boldsymbol{H}_{n+1} = H_1\boldsymbol{E}^1$ (constant).Set

$$\bar{\boldsymbol{F}}_{n+1} = \bar{\boldsymbol{F}}_n$$

and

2. Calculate the total deformation as

$$\boldsymbol{F}_{n+1} = F_{n+1}\boldsymbol{e}_1 \otimes \boldsymbol{E}^1 + \bar{\boldsymbol{F}}_{n+1}$$

3. Calculate the algorithmic stresses and moduli from the material routine (three dimensional)

$$\begin{aligned} \boldsymbol{P}^t_{n+1} &= \hat{\boldsymbol{P}}^t(\boldsymbol{F}_{n+1}, \boldsymbol{H}_{n+1}) \\ \mathbb{A}_{n+1} &= \partial_{\boldsymbol{F}_{n+1}}\hat{\boldsymbol{P}}(\boldsymbol{F}_{n+1}, \boldsymbol{H}_{n+1}) \end{aligned}$$

4. Extract the stress and moduli for the transverse part

$$\begin{aligned} \bar{\boldsymbol{P}}^t_{n+1} &= \boldsymbol{P}^t - P_{n+1}\boldsymbol{e}_1 \otimes \boldsymbol{E}_1 \\ \bar{\mathbb{A}}_{n+1} &= \partial_{\bar{\boldsymbol{F}}_{n+1}}\bar{\boldsymbol{P}}(\boldsymbol{F}_{n+1}, \boldsymbol{H}_{n+1}) \end{aligned}$$

5. Update the transverse deformation as

$$\bar{\boldsymbol{F}}_{n+1} \Leftarrow \bar{\boldsymbol{F}}_{n+1} - \bar{\mathbb{A}}^{-1}_{n+1} : \bar{\boldsymbol{P}}_{n+1}$$

6. Check for Convergence. If ($\|\boldsymbol{P}^t_{n+1}\| \geq tol$) go to 2.

Box 3: Driver algorithm for simple tension.

6.1.2.2. Transversely-Isotropic Material Model. Similar to the shear test response, the relative directions of the chains and the magnetic field determine the extent of the magneto-mechanical coupling. When they are perpendicular to one another the coupling is absent. The values of bulk and shear modulus are 10.0N/mm^2 and 5.0N/mm^2 respectively, while the values of c_1 and c_2 and c_3 are the same as before. while the plots are in Figure 22.

6.1.2.3. Saturation Type Material Model. Once again, since the above models do not capture the *saturation effect* on stiffening response of the material, we look at the *Saturation type model*. It can be seen in Figure 24 that the saturation effect is captured since the plots of stress vs. strain are apart for the lower values of magnetic field but then almost coincide for the higher magnetic fields. The material parameters are the same as before.

It is important to note that the material parameters have been chosen after a parameter identification process using a *Sequential Quadratic Programming* (SQP) algorithm for

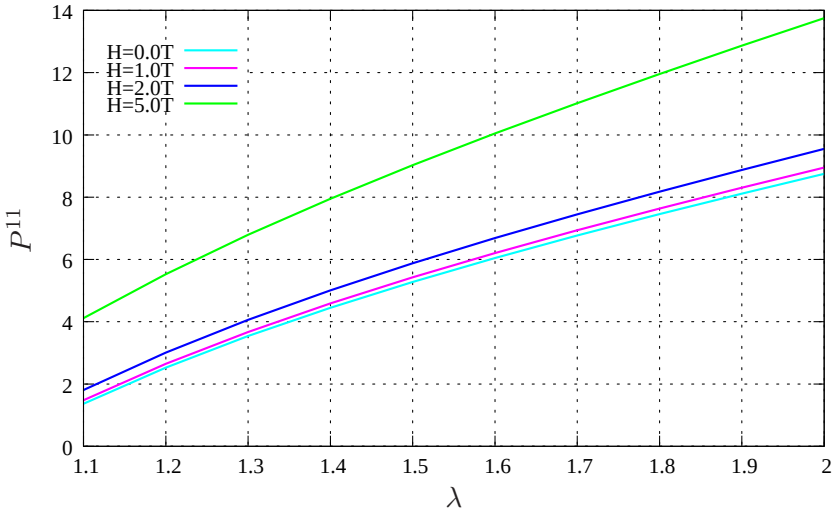

Figure 21: Simple tension of Neo-hookean material model solicited in the direction of the magnetic field

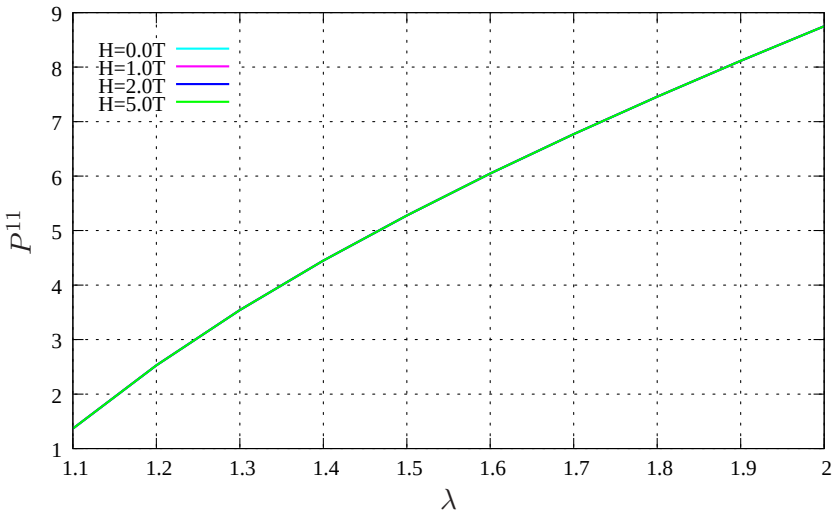

Figure 22: Simple tension of transversely anisotropic material model solicited in the two different directions with respect to the magnetic field. Chains aligned perpendicular to magnetic field

constrained optimization. This way, we may emphasize that the results obtained, capture the real response of the material not only qualitatively but also *quantitatively*.

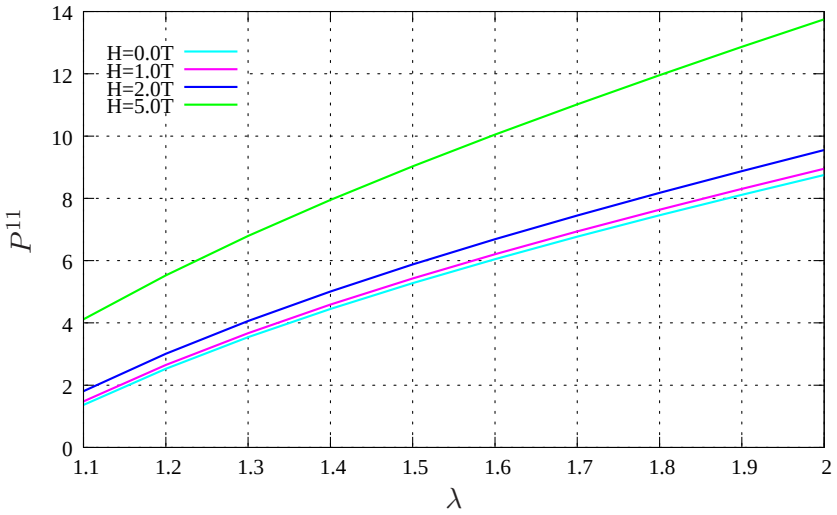

Figure 23: Simple tension of Transversely anisotropic material model solicited in the two different directions with respect to the magnetic field. Chains aligned parallel to magnetic field

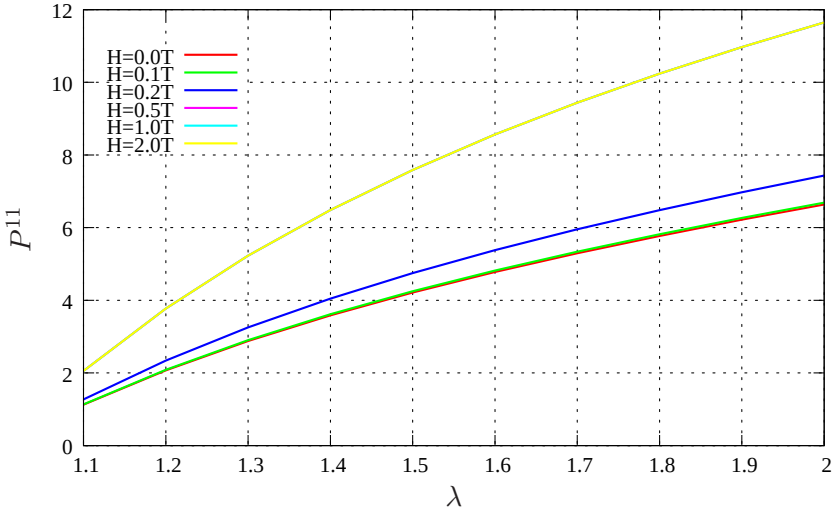

Figure 24: Simple tension of Saturation type material model.

6.2. Selected Boundary Value Problems

6.2.1. Shear test at constant reference magnetic field. Literature on the on the characteristics of magnetostrictive elastomers although scarce, primarily focusses on the change in shear modulus of a specimen with magnetic field. For example, Figure 3 in Section 2 taken from JOLLY ET AL [17] shows (a) the experimental setup used for measuring change in shear modulus, and (b) the result obtained for one of the double lap shear specimens. Here, the specimen, sandwiched between two plates is subjected to a shear deformation while a magnetic field is applied in the vertical direction.

The above motivates us to consider a boundary value problem of the type shown in Figure 25. Here, we specified displacement on the upper and lower edges and a constant potential difference is applied across these two edges. The results of the Finite Element simulation for potential differences of $\Delta\Phi = \{1 \times 798.5\,\text{A},\ 2 \times 798.5\,\text{A} \text{ and } 5 \times 798.5\,\text{A}\}$ are displayed in Figure 26. The values of $\Delta\Phi$ used in the simulation are chosen such that they, correspond to magnetic field strengths of $\boldsymbol{H} \approx \{0.1\,\text{T},\ 0.2\,\text{T}, \text{and } 0.5\,\text{T}\}$.

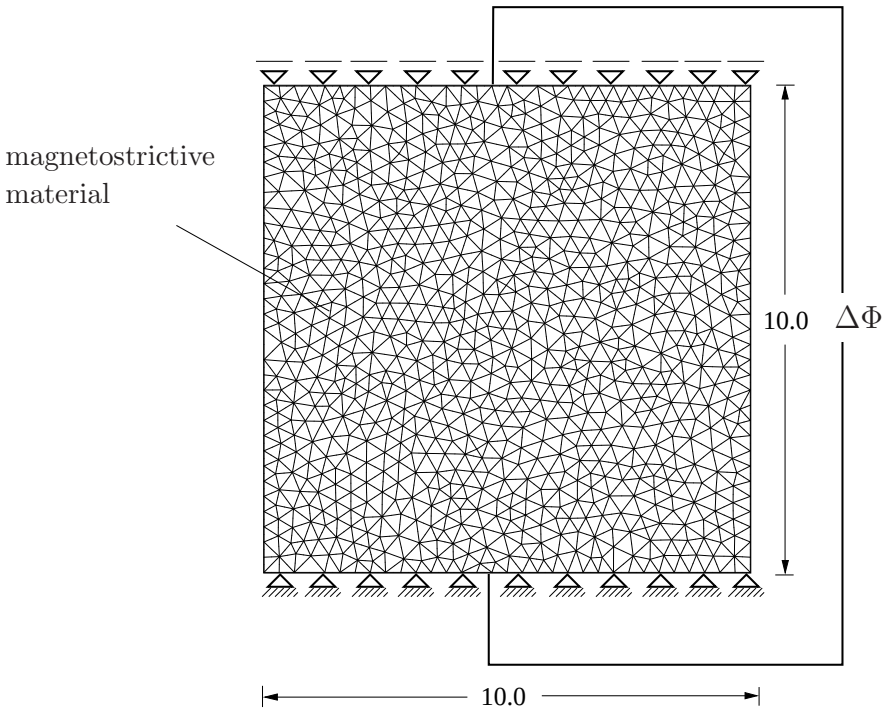

Figure 25: Definition of the boundary value problem to study shear stress distribution of the magnetostrictive block deformed in the presence of a constant magnetic field. All dimensions are in mm and $\bar{u}_x = 1.0\,\text{mm}$

Figure 26 shows the results of the Finite Element simulation where the material is modeled with the *isotropic Neo-Hookean-type free energy-enthalpy function*. The shear stress distribution is displayed at three different magnetic fields. It is clearly observed that *higher shear stresses* result from *higher magnetic fields*. Physically, this is the expected response since on increasing the applied magnetic field, the magnetization of the iron particles embedded within the matrix increases. This results in *increased magnetic forces of attraction* between particles that *stiffens* the material resulting in greater stresses for the same deformation.

From a modeling viewpoint, a higher magnetic field raises the free energy-enthalpy

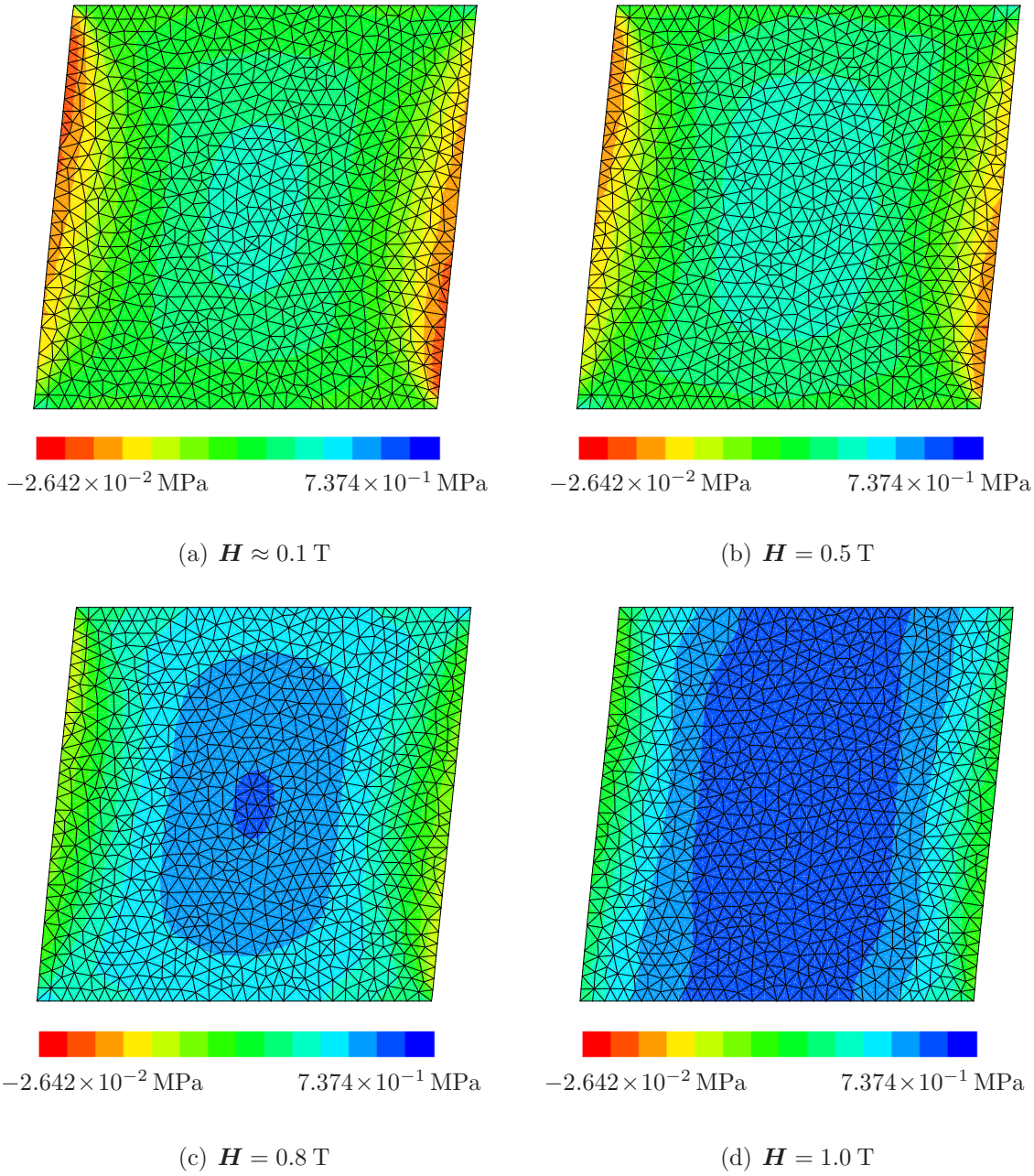

(a) $\boldsymbol{H} \approx 0.1$ T (b) $\boldsymbol{H} = 0.5$ T

(c) $\boldsymbol{H} = 0.8$ T (d) $\boldsymbol{H} = 1.0$ T

Figure 26: Finite element simulation results for shear of block of Neo-Hookean type material. The above are the plots of shear stress $P^{12,t}$ at different magnetic field strengths.

(81) of the material and similarly, the stress expression defined by (82a) shows that the stress must increase. This is also in accordance with the driver test for shear deformation in the previous subsection.

6.2.2. Magnetostrictive Material in Free Space. Boundary conditions play a very important role in Thermo-Magneto-Mechanical experiments. Kiefer, Karaca, Lagoudas & Karaman [20] describes an experimental setup for studying magnetostrictive materials. In reality, magnetic boundary conditions are not applied on the surface of the material but rather, in the adjoining 'free-space' as explained in Section 2.3.

This motivates to also model the free space surrounding the material in our boundary

value problem and apply the boundary conditions on this free space rather than directly on the material domain. The free-space is modeled as a material with *very low elastic stiffness*- of four orders of magnitude lower than that of the magnetostrictive material. In the boundary value problem presented below we have a magnetostrictive material surrounding a hard inclusion which is placed in a 'free-space box'.

The results of the simulation are shown in Figure 28 where we have used the isotropic Neo-Hookean-type free energy enthalpy function and we can see that the magnetostrictive material shrinks around the hard inclusion due to the magnetic field. This simulation

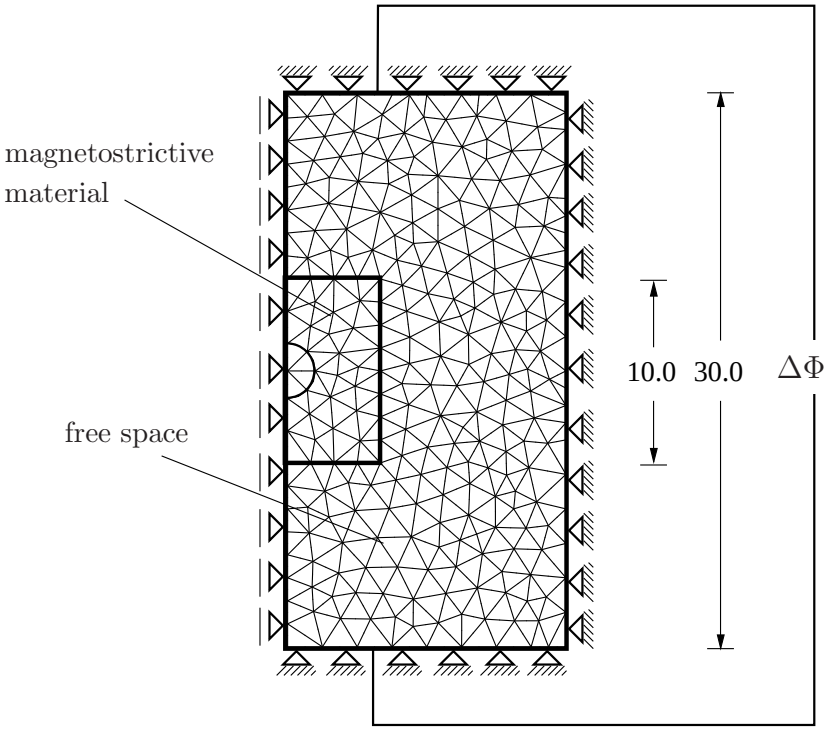

Figure 27: Definition of the boundary value problem with free space. Symmetry of the problem is exploited so as to compute the solution on the shown 'half mesh' and results are mirrored on the symmetry axis.

shows a more realistic solution in the sense of the boundary conditions being applied.

6.2.3. Magnetostrictive Material for varying the stiffness of a suspension bushing. A bushing is a type of bearing or a cylindrical lining designed to constrict motion of mechanical parts. A recent application of magnetostrictive materials is in imparting an increased *controllable stiffness* to bushings as described by Watson [34]. Here, a magnetostrictive elastomer is interposed between the inner and outer cylinders of the bushing and a coil is disposed about the inner cylinder . When the coil is energized by electrical current a magnetic field is generated under whose influence, the stiffness of the magnetostrictive material changes which means that the bushing is imparted a variable stiffness. In order to model a similar situation, we have the boundary problem as shown in the following figure. We now solve the problem for *two cases*. In the *first case*, there is no magnetic field while in the *second case*, the magnetic field is applied in the *y-direction*. In both cases a force in the y-direction has been applied at the center of the rigid circle

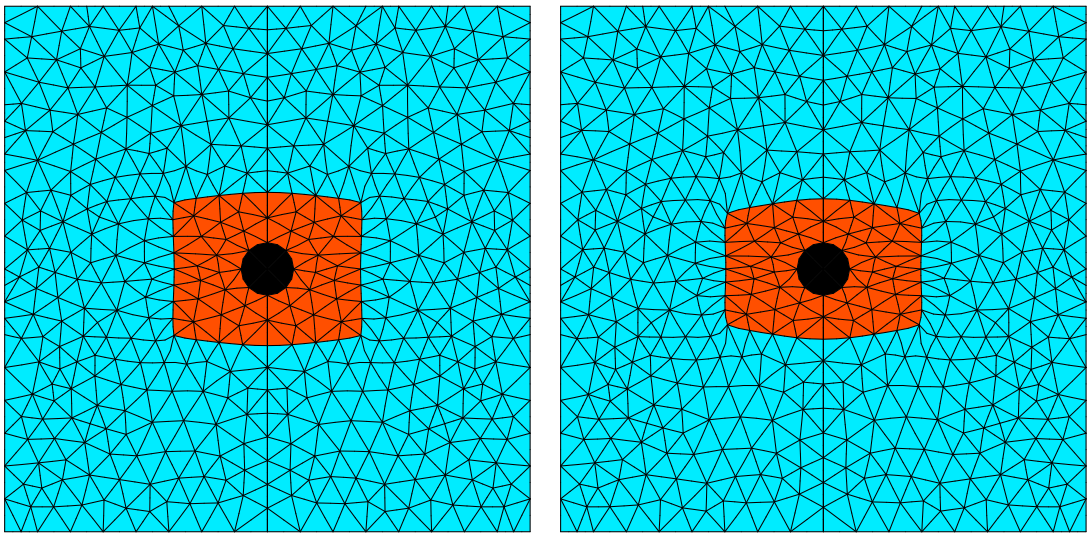

(a) Deformation at $\boldsymbol{H} \approx 1.0\,\mathrm{T}$

(b) Deformation at $\boldsymbol{H} \approx 1.5\,\mathrm{T}$

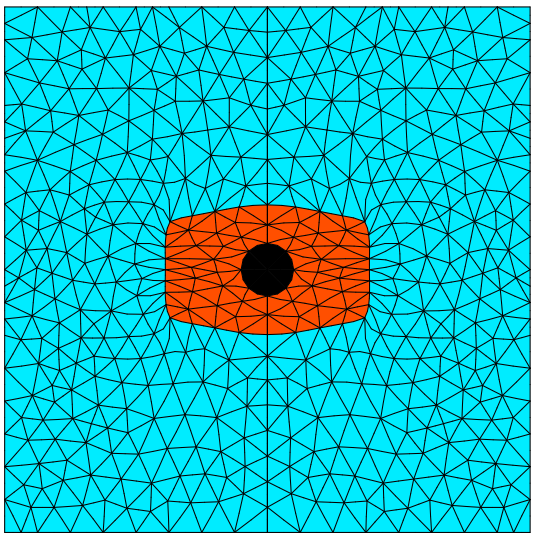

(c) Deformation at $\boldsymbol{H} \approx 2.0\,\mathrm{T}$

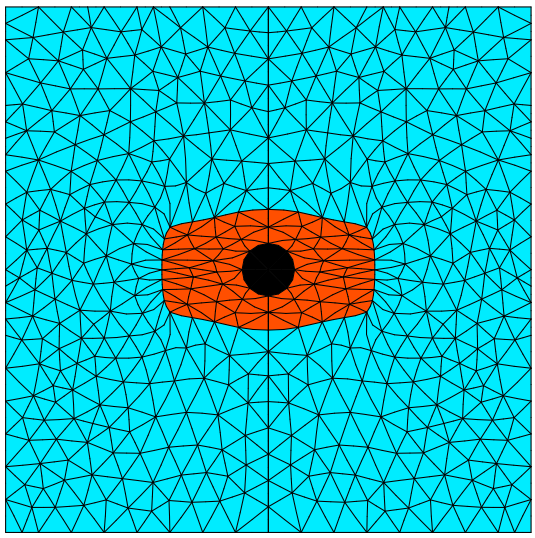

(d) Deformation at $\boldsymbol{H} \approx 2.5\,\mathrm{T}$

Figure 28: Finite element simulation results at different magnetic fields of the deformed mesh for magnetostrictive material with a hard inclusion in free-space. Symmetry has been exploited to show results.

as shown in Figure 29.

The mesh when deformed to the maximum extent for both cases has been shown in Figure 30. The simulation gives the expected results. In the presence of the magnetic field, the increased stiffness of the material causes the mesh deform to a lesser extent than it does when the magnetic field is zero.

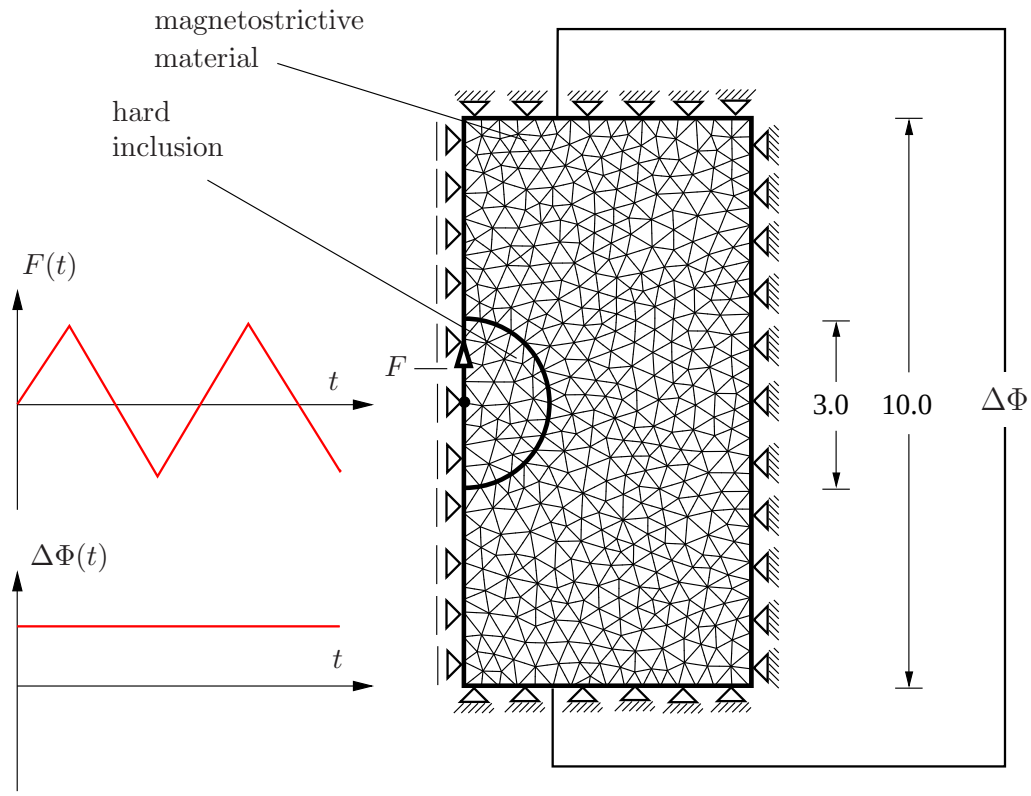

Figure 29: Mesh and definition of the boundary value problem. A force is applied at the center of the hard circular inclusion in a cyclic manner as shown in the figure.

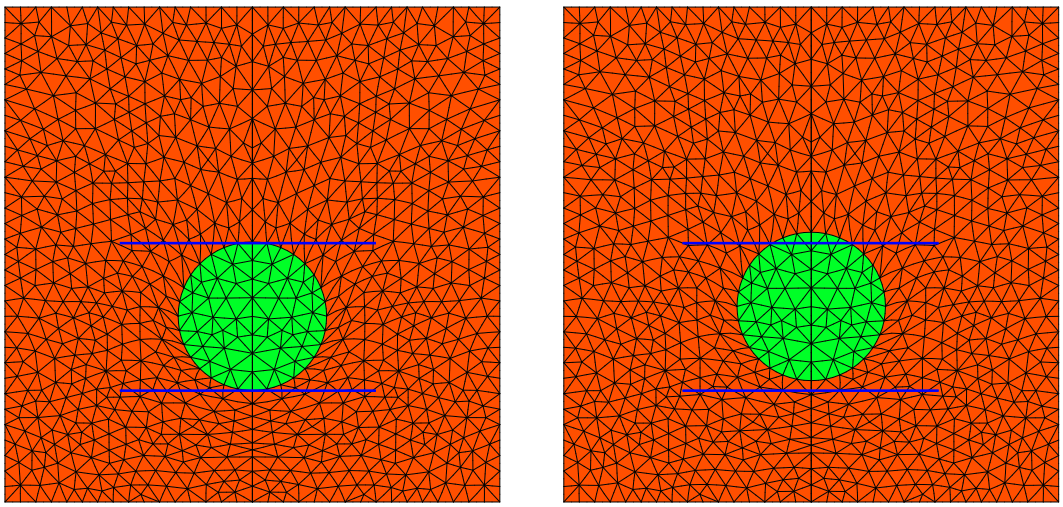

Figure 30: Finite element simulation results of the deformed configuration at (a) no magnetic field and (b) magnetic field of approximately 0.03 T

6.2.4. Bi-Material (Finger) Actuator. Another use of magnetostrictives materials is in the field of robotics. Since these materials deform on the application of magnetic field, they may be used in making finger actuators. Typically deformations in such applications are large and this is an area where finite strain modeling is required. In the example that follows, we model a finger as a composite bar and show how the bar deforms under application of magnetic fields. The example shows that finite strain modeling is indeed a requirement from a practical perspective.

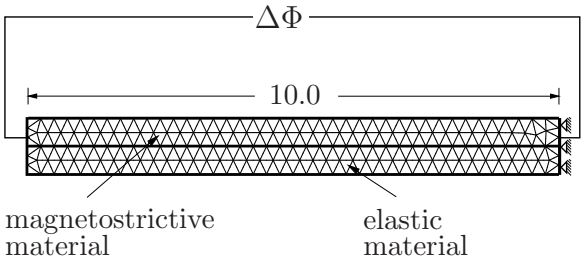

Figure 31: Mesh and definition of the boundary value problem. A monotonically increasing magnetic potential difference $\Delta\Phi$ is applied between the ends of the composite bar and the displacements at the right end are fixed.

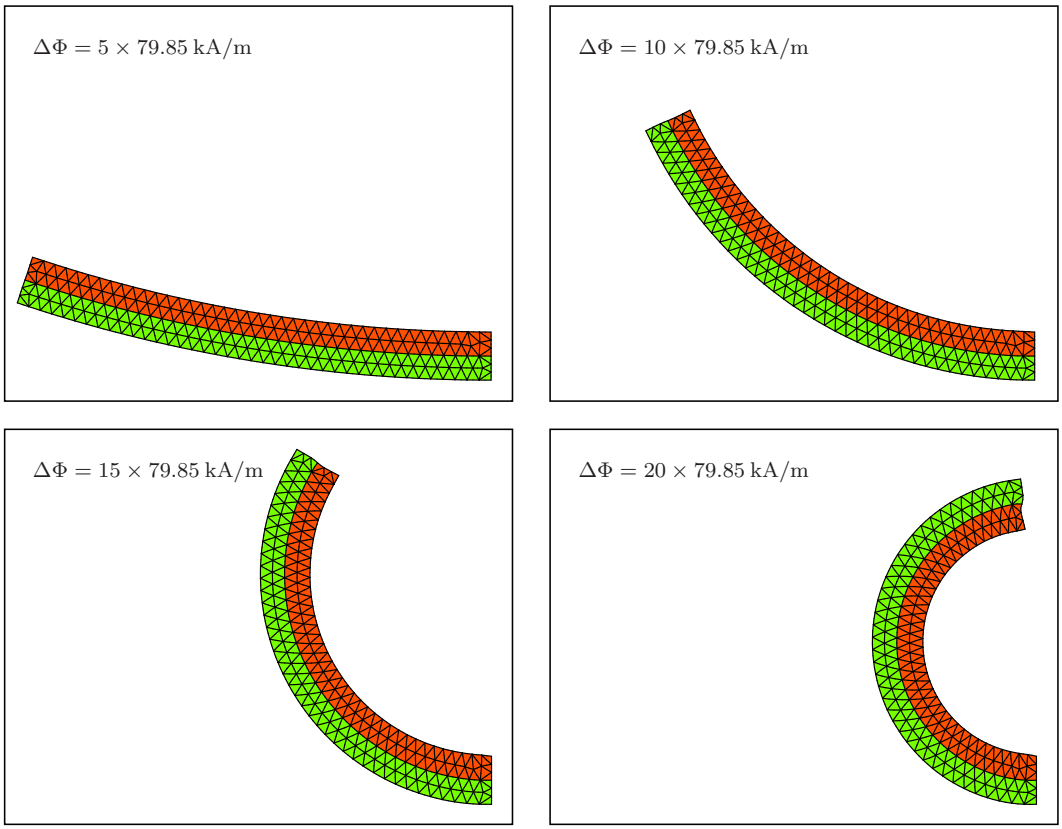

Figure 32: Deformed configurations of the composite bar at different applied potential differences $\Delta\Phi$.

7. Conclusions

In the work presented, a consistent finite deformation framework for the description of magnetizable continua was derived with a focus on the fundamental geometric mappings of mechanical and magnetic field variables, extended balance laws and Maxwell's equations, magnetic body force, couple and energy source terms and Maxwell's stress tensor concept, boundary and jump conditions, magnetic potentials and variational formulation of the fully coupled problem.

Additionally, a discussion of constitutive theory for finite magnetostriction was presented with the key aspects being thermodynamic consistency, choice of thermodynamic potential, objectivity, material symmetry, geometrical and physical nonlinearities, and anisotropy. With this as background, three different models- *an extended compressible Neo-Hookean model, an anisotropic compressible extended Neo-Hookean model* and *an isotropic model with saturation of the magnetomechanical coupling effect* have been presented so as to successfully capture the main features of magnetorheological elastomers. We have also presented driver algorithms for observing the response of the proposed material models to simple tension and shear tests. To this end, we have also shown in the internship report with the title *Implementation of a Parameter Identification Algorithm for Finite Magnetostriction Models*, how the driver algorithms are used in a nonlinear optimization algorithm in order to obtain an optimal set of parameters to fit experimental data.

Finally, finite element solutions of technologically relevant fully-coupled two-dimensional boundary value problems have been presented and discussed.

References

[1] Boehler, J. P. (Editor) [1987]: *Applications of Tensor Functions in Solid Mechanics*, Vol. 292 of *CISM Courses and Lectures*. Springer-Verlag, Wien, New York.

[2] Bowen, R. B. [1989]: *Introduction to Continuum Mechanics for Engineers*. Plenum Press, New York.

[3] Brigadnov, I. A.; Dorfmann, A. [2003]: *Mathematical Modeling of Magneto-Sensitive Elastomers*. International Journal of Solids and Structures, 40: 4659–4674.

[4] Bustamante, R.; Dorfmann, A.; Odgen, R. W. [2007]: *A Nonlinear Magnetoelastic Tube Under Extension and Inflation in an Axial Magnetic Field: Numerical Solution*. Journal of Engineering Mathematics, 59: 139–153.

[5] Coleman, B. D.; Noll, W. [1963]: *The Thermodynamics of Elastic Materials with Heat Conduction and Viscosity*. Archive for Rational Mechanics and Analysis, 13: 167–178.

[6] Davis, L. C. [1999]: *Model of Magnetorheological Elastomers*. Journal of Applied Physics, 85(6): 3348–3351.

[7] Devonshire, A. F. [1954]: *Theory of Ferroelectrics*. Advances in Physics, 3(10): 85–130.

[8] Dixon, R. C.; Eringen, A. C. [1964]: *A Dynamical Theory of Polar Elastic Dielectrics I*. International Journal of Engineering Science, 3: 359–377.

[9] Dixon, R. C.; Eringen, A. C. [1964]: *A Dynamical Theory of Polar Elastic Dielectrics II*. International Journal of Engineering Science, 3: 379–398.

[10] Dorfmann, A.; Ogden, R. W. [2003]: *Magnetoelastic Modelling of Elastomers*. European Journal of Mechanics A/Solids, 22: 497–507.

[11] Dorfmann, A.; Ogden, R. W. [2004]: *Nonlinear Magnetoelastic Deformations*. The Quaterly Journal of Mechanics and Applied Mathematics, 57(4): 599–622.

[12] Dorfmann, A. L.; Ogden, R. W. [2009]: *Electromagnetism: from Basic Principles to the Analysis of Nonlinear Interactions in Deformable Media*. In Ogden, R. W.; Steigmann, D. J. (Editors): *Mechanics and Electrodynamics of Magneto- and Electro-elastic Materials*, Vol. to appear of *CISM Courses and Lectures*. Springer-Verlag, Wien, New York.

[13] Eringen, A. C.; Maugin, G. A. [1990]: *Electrodynamics of Continua I — Foundations and Solid Media*. Springer-Verlag, New York.

[14] Gurtin, M. E. [1981]: *An Introduction to Continuum Mechanics*, Vol. 158. Academic Press, San Diego.

[15] Hutter, K.; Ven, A. A. F. van de [1978]: *Field Matter Interactions in Thermoelastic Solids*, Vol. 88 of *Lecture Notes in Physics*. Springer-Verlag, New York.

[16] Jackson, J. D. [1975]: *Classical Electrodynamics*. John Wiley & Sons, New York, 2nd Edition.

[17] Jolly, M. R.; Carlson, D.; Muñoz, B. C.; Bullions, T. A. [1996]: *The Magnetoviscoelastic Response of Elastomer Composites Consisting of Ferrous Particles Embedded in a Polymer Matrix*. Journal of Intelligent Material Systems and Structures, 7: 613–622.

[18] Kallio, M. [2005]: *The Elastic and Damping Properties of Magnetorheological Elastomers*. Ph.D. Dissertation, Tampere University of Technology.

[19] Kankanala, S. V.; Triantafyllidis, N. [2004]: *On Finitely Strained Magnetorheological Elastomers*. Journal of Mechanics and Physics of Solids, 52: 2869–2908.

[20] Kiefer, B.; Karaca, H. E.; Lagoudas, D. C.; Karaman, I. [2007]: *Characterization and Modeling of the Magnetic Field-Induced Strain and Work Output in* Ni_2MnGa *Shape Memory Alloys*. Journal of Magnetism and Magnetic Materials, 312(1): 164–175.

[21] Kiefer, B.; Rosato, D.; Miehe, C. [2007]: *On the Modeling of Thermo-Electro-Magneto-Mechanical Solids at Finite Strains*. PAMM Proceedings in Applied Mathematics and Mechanics, 7(1): 4070025–4070026.

[22] Kiefer, B.; Rosato, D.; Miehe, C. [2009]: *Geometrical Aspects of the Incorporation of Free Space in Magnetomechanics at Finite Strains*. PAMM Proceedings in Applied Mathematics and Mechanics, to appear.

[23] Lorentz, H. A. [1900]: *Theory of Electrons*. Dover Publications, New York, Reprint (1952) Edition.

[24] Marsden, J. E.; Hughes, T. J. R. [1983]: *Mathematical Foundations of Elasticity*. Prentice Hall, Englewood Cliffs, NJ.

[25] Maugin, G. A. [1988]: *Continuum Mechanics of Electromagnetic Solids*, Vol. 33 of *North-Holland Series in Applied Mathematics and Mechanics*. Elsevier Science Publishers, Amsterdam.

[26] Pao, Y.-H. [1978]: *Electromagnetic Forces in Deformable Continua*. In Nemat-Nasser, S. (Editor): *Mechanics Today*, Vol. 4, Chapter 4, pp. 209–305. Pergamon Press, New York. Published on behalf of the American Academy of Mechanics.

[27] Pao, Y. H.; Hutter, K. [1975]: *Electrodynamics for Moving Elastic Solids and Viscous Fluids*. Proceedings of the IEEE, 63(7): 1011–1021.

[28] Penfield Jr., P.; Haus, H. A. [1967]: *Electrodynamics of Moving Media*, Vol. 40 of *Research Monographs*. M. I. T. Press, Cambridge, MA.

[29] Semenov, A. S.; Kessler, H.; Liskowsky, A.; Balke, H. [2006]: *On a Vector Potential Formulation for 3D Electromechanical Finite Element Analysis*. Communications in Numerical Methods in Engineering, 22: 357–375.

[30] Steigmann, D. J. [2004]: *Equilibrium Theory for Magnetic Elastomers and Magnetoelastic Membranes*. International Journal of Non-Linear Mechanics, 39: 1193–1216.

[31] Varga, Z.; Filipcsei, G.; Zrínyi, M. [2005]: *Smart Composites with Controlled Anisotropy*. Polymer, 46: 7779–7787.

[32] Varga, Z.; Filipcsei, G.; Zrínyi, M. [2006]: *Magnetic Field Sensitive Functional Elastomers with Tuneable Elastic Modulus*. Polymer, 47: 227–233.

[33] Vu, D. K.; Steinmann, P.; Possart, G. [2007]: *Numerical Modelling of Non-Linear Electroelasticity*. International Journal for Numerical Methods in Engineering, 70: 685–704.

[34] Watson, J.R. [1996]: *Method and Apparatus for Varying the Stiffness of a Suspension Bushing*. United States Patent 5,609,353, Ford Motor Company.

A. Additional Derivations

A.1. The Euler-Lagrange Equations of the Variational Problem (56)

The starting point is the necessary condition for stationarity of the variational problem, expression (57)

$$\delta I(\boldsymbol{\varphi}, \delta\boldsymbol{\varphi}, -\Phi, \delta(-\Phi)) = \int_{\mathcal{B}} \left[\partial_{\boldsymbol{F}} \hat{\psi}^* : \operatorname{Grad} \delta\boldsymbol{\varphi} + \partial_{\boldsymbol{H}} \hat{\psi}^* \cdot \operatorname{Grad} \delta(-\Phi) \right] dV$$
$$- \int_{\partial\mathcal{B}_t} \bar{\boldsymbol{t}}^t \cdot \delta\boldsymbol{\varphi} \, dA + \int_{\partial\mathcal{B}_B} \bar{B} \cdot \delta(-\Phi) \, dA \stackrel{!}{=} 0 \, .$$

Using the identities

$$\partial_{\boldsymbol{F}} \hat{\psi}^* : \operatorname{Grad} \delta\boldsymbol{\varphi} = \operatorname{Div} \left[\left(\partial_{\boldsymbol{F}} \hat{\psi}^* \right)^T \delta\boldsymbol{\varphi} \right] - \operatorname{Div} \left[\partial_{\boldsymbol{F}} \hat{\psi}^* \right] \cdot \delta\boldsymbol{\varphi} \, , \tag{101}$$

$$\partial_{\boldsymbol{H}} \hat{\psi}^* \cdot \operatorname{Grad} \delta(-\Phi) = \operatorname{Div} \left[\delta(-\Phi) \, \partial_{\boldsymbol{H}} \hat{\psi}^* \right] - \delta(-\Phi) \operatorname{Div} \left[\partial_{\boldsymbol{H}} \hat{\psi}^* \right] \, , \tag{102}$$

and subsequently applying the divergence theorem, it follows for the first term on the right hand side of the stationarity condition, which we denote as T1

$$\mathrm{T1} = \int_{\mathcal{B}} \Big\{ \operatorname{Div} \left[\left(\partial_{\boldsymbol{F}} \hat{\psi}^* \right)^T \delta\boldsymbol{\varphi} \right] - \operatorname{Div} \left[\partial_{\boldsymbol{F}} \hat{\psi}^* \right] \cdot \delta\boldsymbol{\varphi} + \operatorname{Div} \left[\delta(-\Phi) \, \partial_{\boldsymbol{H}} \hat{\psi}^* \right]$$
$$- \delta(-\Phi) \operatorname{Div} \left[\partial_{\boldsymbol{H}} \hat{\psi}^* \right] \Big\} \, dV \, , \tag{103}$$
$$= \int_{\partial\mathcal{B}} \left\{ \left(\partial_{\boldsymbol{F}} \hat{\psi}^* \right)^T \delta\boldsymbol{\varphi} + \delta(-\Phi) \, \partial_{\boldsymbol{H}} \hat{\psi}^* \right\} \cdot \boldsymbol{N} \, dA$$
$$- \int_{\mathcal{B}} \left\{ \operatorname{Div} \left[\partial_{\boldsymbol{F}} \hat{\psi}^* \right] \cdot \delta\boldsymbol{\varphi} + \operatorname{Div} \left[\partial_{\boldsymbol{H}} \hat{\psi}^* \right] \delta(-\Phi) \right\} \, dV \, .$$

The above stationarity condition can thus be rewritten as

$$\delta I = \int_{\partial\mathcal{B}_t} \left[\left(\partial_{\boldsymbol{F}} \hat{\psi}^* \right) \boldsymbol{N} - \bar{\boldsymbol{t}}^t \right] \cdot \delta\boldsymbol{\varphi} \, dA + \int_{\partial\mathcal{B}_B} \left[\left(\partial_{\boldsymbol{H}} \hat{\psi}^* \right) \cdot \boldsymbol{N} + \bar{B} \right] \delta(-\Phi) \, dA \tag{104}$$
$$- \int_{\mathcal{B}} \operatorname{Div} \left[\partial_{\boldsymbol{F}} \hat{\psi}^* \right] \cdot \delta\boldsymbol{\varphi} \, dv - \int_{\mathcal{B}} \operatorname{Div} \left[\partial_{\boldsymbol{H}} \hat{\psi}^* \right] \delta(-\Phi) \, dV \stackrel{!}{=} 0 \, .$$

Since the necessary condition (104) must hold for all admissible $\delta\boldsymbol{\varphi}$ and $\delta(-\Phi)$, one obtains the following local expressions

$$\operatorname{Div} \left[\partial_{\boldsymbol{F}} \hat{\psi}^* \right] = \boldsymbol{0} \quad \text{in } \mathcal{B} \, , \qquad \left(\partial_{\boldsymbol{F}} \hat{\psi}^* \right) \boldsymbol{N} = \bar{\boldsymbol{t}}^t \quad \text{on } \partial\mathcal{B}_t \, , \tag{105a}$$

$$\operatorname{Div} \left[\partial_{\boldsymbol{H}} \hat{\psi}^* \right] = 0 \quad \text{in } \mathcal{B} \, , \qquad \left(\partial_{\boldsymbol{H}} \hat{\psi}^* \right) \cdot \boldsymbol{N} = -\bar{B} \quad \text{on } \partial\mathcal{B}_B \, . \tag{105b}$$

In the terminology of variational calculus relations (105) are the *Euler-Lagrange equations* of the variational problem (56) and include the *natural boundary conditions* of the variational problem. Expressions (105) are identical with the equilibrium equations and boundary conditions (55) specified in Section 3.5, Box 1. Note that in the above derivation the mechanical body force term has been excluded for conciseness. The appropriate jump conditions over discontinuity surfaces (55e) may also directly be deduced from the variational problem by applying an extended form of the divergences theorem (see e.g. [2]).